

AD-A185 782 NITROGEN SCALE-UP(U) TRM SPACE AND TECHNOLOGY GROUP
REDONDO BEACH CA J A BETTS ET AL JUN 87 AFML-TR-86-83
F29681-84-C-0074

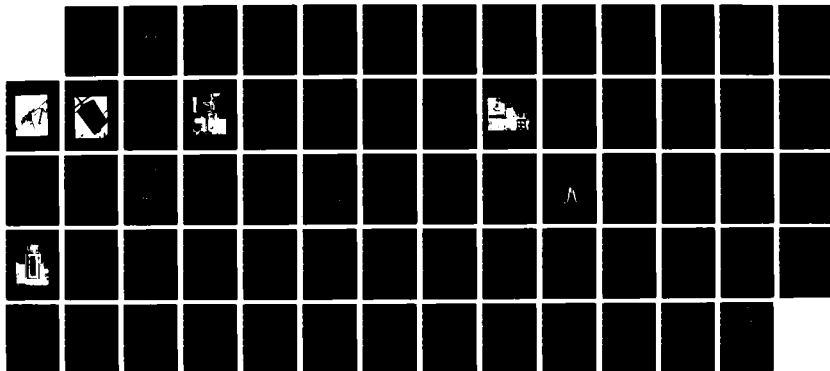
NITROGEN SCALE-UP(U) TRW SPACE AND TECHNOLOGY GROUP
REDONDO BEACH CA J A BETTS ET AL JUN 87 AFHL-TR-86-03
F29601-84-C-0074

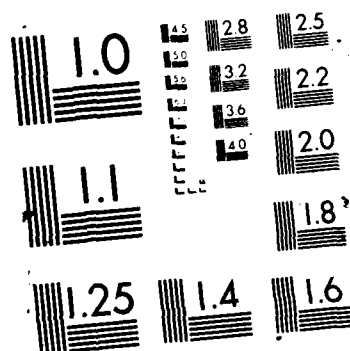
14

UNCLASSIFIED

F/8 2/3

14

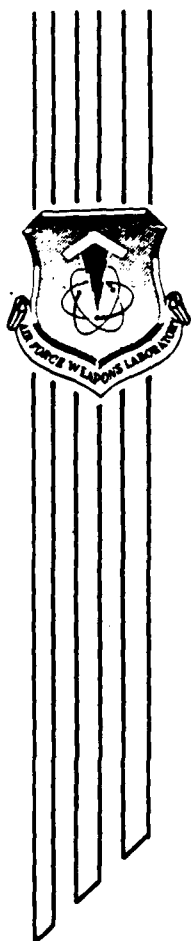




9713 FILE COPY

DTIC
ELECTE
OCT 15 1987

AIR FORCE WEAPONS LABORATORY
Air Force Systems Command
Kirtland Air Force Base, NM 87117-6008



This final report was prepared by TRW Space and Technology Group, Redondo Beach, California under Contract F29601-84-C-0074, Job Order 33261W11. Dr Yolanda Jones (ARDA) was the Laboratory Project Officer-in-Charge.

When Government drawings, specifications, or other data are used for any purpose other than in connection with a definitely Government-related procurement, the United States Government incurs no responsibility or any obligation whatsoever. The fact that the Government may have formulated or in any way supplied the said drawings, specifications, or other data, is not to be regarded by implication, or otherwise in any manner construed, as licensing the holder, or any other person or corporation; or as conveying any rights or permission to manufacture, use, or sell any patented invention that may in any way be related thereto.

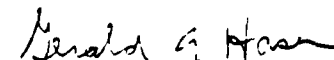
This report has been authored by a contractor of the United States Government. Accordingly, the United States Government retains a nonexclusive, royalty-free license to publish or otherwise reproduce the material contained herein, or allow others to do so, for United States Government purposes.

This report has been reviewed by the Public Affairs Office and is releasable to the National Technical Information Service (NTIS). At NTIS, it will be available to the general public, including foreign nations.

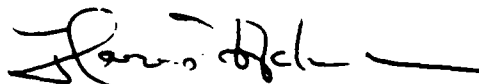
If your address has changed, if you wish to be removed from our mailing list, or if your organization no longer employs the addressee, please notify AFWL/ARDA, Kirtland AFB, NM 87117-6008 to help us maintain a current mailing list.

This technical report has been reviewed and is approved for publication.


YOLANDA JONES, PhD
Project Officer


GERALD A. HASEN
Major, USAF
Chief, Advanced Chemical Laser Br

FOR THE COMMANDER


HARRO ACKERMANN
Lt Col, USAF
Chief, Laser Science & Technology Ofc

DO NOT RETURN COPIES OF THIS REPORT UNLESS CONTRACTUAL OBLIGATIONS OR NOTICE ON A SPECIFIC DOCUMENT REQUIRES THAT IT BE RETURNED.

REPORT DOCUMENTATION PAGE

1a. REPORT SECURITY CLASSIFICATION UNCLASSIFIED			1b. RESTRICTIVE MARKINGS		
2a. SECURITY CLASSIFICATION AUTHORITY			3. DISTRIBUTION/AVAILABILITY OF REPORT Approved for public release; distribution unlimited.		
2b. DECLASSIFICATION/DOWNGRADING SCHEDULE					
4. PERFORMING ORGANIZATION REPORT NUMBER(S)			5. MONITORING ORGANIZATION REPORT NUMBER(S) AFWL-TR-86-03		
6a. NAME OF PERFORMING ORGANIZATION TRW Space & Technology Group		6b. OFFICE SYMBOL (If applicable)	7a. NAME OF MONITORING ORGANIZATION Air Force Weapons Laboratory		
6c. ADDRESS (City, State and ZIP Code) One Space Park Redondo Beach, CA 90278			7b. ADDRESS (City, State and ZIP Code) Kirtland Air Force Base, NM 87117-6008		
8a. NAME OF FUNDING/SPONSORING ORGANIZATION		8b. OFFICE SYMBOL (If applicable)	9. PROCUREMENT INSTRUMENT IDENTIFICATION NUMBER F29601-84-C-0074		
8c. ADDRESS (City, State and ZIP Code)			10. SOURCE OF FUNDING NOS.		
			PROGRAM ELEMENT NO. 62601F	PROJECT NO. 3326	TASK NO. 1W
					WORK UNIT NO. 11
11. TITLE (Include Security Classification) NITROGEN SCALE-UP					
12. PERSONAL AUTHOR(S) Betts, Jeanette A.; and Fukumoto, Joseph M.					
13a. TYPE OF REPORT Final		13b. TIME COVERED FROM 9Sep84 to 2Sep 85		14. DATE OF REPORT (Yr., Mo., Day) 1987 June	
				15. PAGE COUNT 68	
16. SUPPLEMENTARY NOTATION					
17. COSATI CODES			18. SUBJECT TERMS (Continue on reverse if necessary and identify by block number)		
FIELD	GROUP	SUB GR			
07	04		Active nitrogen H/NF ₂ chemistry N ₂ (A) formation Chemically reactive flows		
19. ABSTRACT (Continue on reverse if necessary and identify by block number) Experiments are described which investigated the Continuous Wave (CW) scaling of excited nitrogen production in an H/NF ₂ reaction system. The purpose is to assess the potential for the development of an electronic transition chemical laser using N ₂ (A) as an energy transfer donor. The experiments use a chemical laser combustor to produce fluorine atoms which are subsequently mixed with hydrogen to produce H-atoms. Heated tetrafluorohydrazine is subsequently mixed in the stream through a HYLITE nozzle to initiate the H/NF ₂ chemistry. In a second series of experiments, NF ₃ was burned in the combustor to produce NF ₂ and F-atoms which were then mixed with H ₂ to initiate the desired chemistry. Relatively low yields of excited nitrogen were obtained in all experiments. The highest observed densities were of the order of 10 ¹² N ₂ (A) and N ₂ (B). Parametric plots used to optimize the system are presented.					
20. DISTRIBUTION/AVAILABILITY OF ABSTRACT UNCLASSIFIED/UNLIMITED <input checked="" type="checkbox"/> SAME AS RPT <input type="checkbox"/> DTIC USERS <input type="checkbox"/>			21. ABSTRACT SECURITY CLASSIFICATION UNCLASSIFIED		
22a. NAME OF RESPONSIBLE INDIVIDUAL Yolanda Jones, PhD			22b. TELEPHONE NUMBER (Include Area Code) (505) 844-1871		22c. OFFICE SYMBOL ARDA

UNCLASSIFIED

SECURITY CLASSIFICATION OF THIS PAGE

UNCLASSIFIED

SECURITY CLASSIFICATION OF THIS PAGE

SUMMARY

A series of tests were run to optimize excited nitrogen production in an H/NF_2 reaction system. In the first series of tests, F-atoms were produced in a chemical laser combustor, reacted with hydrogen in the cavity to produce H-atoms which were reacted with NF_2 radicals to initiate the H/NF_2 chemistry. Yields of $\text{N}_2(\text{A})$ and $\text{N}_2(\text{B})$ were about 10^{-4} of the NF_2 flow. It was found that the excited nitrogen emission intensities were relatively insensitive to any parameters that were varied.

In the second series of tests, an attempt was made to produce NF_2 radicals in the combustor using NF_3 fuel. It appears that the combustor ran cold resulting in little chemistry in the combustor. However, the NF_3 reacted in the cavity to produce intense $\text{N}_2(\text{B})$ emission with high temperatures generated.

Finally, in the third series of tests, NF_3 was added in the cavity in place of N_2F_4 . The $\text{N}_2(\text{B})$ emission resulting from this test indicated that the reaction of H with NF_3 can be sufficiently rapid to initiate the chemistry leading to excited nitrogen production.

Accession For	
NTIS CRA&I	<input checked="" type="checkbox"/>
DTIC TAB	<input type="checkbox"/>
Unannounced	<input type="checkbox"/>
Justification	
By	
Distribution/	
Availability Codes	
Dist	
A-1	



CONTENTS

<u>Section</u>		<u>Page</u>
1	INTRODUCTION	1
2	EXPERIMENTAL	3
	2.1 EXPERIMENTAL APPARATUS	3
	2.1.1 Combustor	3
	2.1.2 Mixing Nozzle	3
	2.1.3 Laser Cavity	3
	2.2 GAS DELIVERY SYSTEM	7
	2.3 OPTICAL DIAGNOSTICS	7
	2.3.1 N ₂ (A) Diagnostic	20
	2.3.2 N ₂ (B) Diagnostic	22
	2.3.3 N ₂ (C) Diagnostic	22
	2.3.4 NF(b) Diagnostic	23
	2.3.5 NF(a) Diagnostic	23
	2.3.6 Temperature Diagnostic	25
	2.4 TEST PROCEDURE	25
3	RESULTS	27
	3.1 SPECTROSCOPY	27
	3.2 DENSITY MEASUREMENTS	30
	3.2.1 F/H ₂ /N ₂ F ₄ Configuration	30
	3.2.2 NF ₃ Based System	41
	3.2.3 H/NF ₃ System	54
4	DISCUSSION OF RESULTS	56
	4.1 H/NF ₂ RESULTS	56
	4.2 NF ₃ BASED SYSTEM	57
	REFERENCES	58

ILLUSTRATIONS

<u>Figure</u>		<u>Page</u>
1	Schematic diagram of system used to study scaling of excited nitrogen production	4
2	Photograph of combustor used to produce F-atoms	5
3	One section of HYLITE nozzle used to mix H_2 and NF_2 with F-atom flow	6
4	Assembled device showing laser cavity	8
5	Peaks in gas chromatograph analysis of N_2F_4 , provided by Hercules	10
6	Photograph of device with attached diagnostics	13
7	Schematic of device showing arrangement of diagnostics	14
8	Optical layout for diagnostics	16
9	Collection Optics	17
10	Experimental layout to verify line of sight effect	18
11	High resolution UV emission spectrum	21
12	Spectrum from 600-1100 nm. Arrows show correction for spectral response of detector	24
13	Ultraviolet emission spectrum from 320 to 350 nm showing $NH(A-X)$ emission	28
14	High resolution ultraviolet emission spectrum from 350 to 390 nm	29
15	Tracor Northern spectrum from 500-800 nm corrected for instrument response	31
16	Photograph of $N_2(B \rightarrow A)$ chemiluminescence	33
17	Plot of $N_2(B)$ emission versus combustor fluorine	34
18	$N_2(B)$ density versus cavity H_2	35
19	Plot of species densities versus X_c for H/NF_2 flame	37
20	Intensity of $N_2(B)$ emission across nozzle. Solid line corresponds to region near nozzle. Dotted line is approximately 10 cm from bottom of nozzle	38

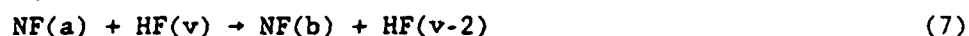
ILLUSTRATIONS (Concluded)

<u>Figure</u>		<u>Page</u>
21	N ₂ (B) intensity versus distance from nozzle. N ₂ (B) optimized near nozzle	42
22	N ₂ (B) versus X_c , N ₂ (B) optimized at $X_c = 7.6$ cm	43
23	N ₂ (B) versus cavity H ₂	44
24	N ₂ (B) versus cavity H ₂	45
25	N ₂ (B) versus F ₂ flow with the F ₂ /H ₂ ratio constant	46
26	N ₂ (B) versus combustor H ₂	47
27	N ₂ (B) density versus cavity pressure	48
28	HF chemiluminescence temperature determination	50
29	Spectra of H ₂ /F ₂ /NF ₃ system showing change in N ₂ (B) vibrational distribution	51
30	NO(A-X) spectrum	53
31	Plots of excited state concentration versus X_c	55

1. INTRODUCTION

Metastable nitrogen, $N_2(A)$, is of interest as an energy storage source and is known to transfer its energy rapidly to several prospective lasing species including the B state of IF and the A state of NO. Thus, demonstration of its production in large quantities could lead to the development of a chemically pumped short wavelength laser.

Excited nitrogen (B→A) emission has been observed in a reaction sequence starting with hydrogen atoms and NF_2 radicals (Ref. 1 through 6). The reaction sequence leading to excited nitrogen production is believed to proceed as follows:



The conventional way to produce hydrogen atoms is by reaction of fluorine atoms, produced in a chemical laser combustor, with hydrogen, i.e.,



Prior interest in this reaction sequence focussed on the production of $NF(a)$ or $NF(b)$ states in hope of producing a directly pumped chemical laser in NF. (Ref. 5 through 6). Consequently, previous scaling studies of this system did not concentrate on the optimization of excited nitrogen even though the nitrogen first positive emission was always present in these studies and sometimes interfered with the $NF(a)$ diagnostic.

The objective of this program was to explore the continuous wave (CW) scaling of $N_2(A)$ production in the H/NF_2 system. The scheme that was studied involved the production of F-atoms in a conventional chemical laser precombustor, mixing these F-atoms with H_2 to produce H-atoms and then mixing the resulting H-atom stream with NF_2 radicals, generated by thermal dissociation of tetrafluorohydrazine (N_2F_4), to initiate the desired chemistry. In addition to the tests performed using N_2F_4 as the NF_2 source, some tests were performed using NF_3 in both the combustor (to directly produce NF_2 radicals) and in the cavity in place of the N_2F_4 .

The main points of the program were: (#1) to utilize existing chemical laser hardware that provided staged injection for mixing reagents in an appropriate manner, and (#2) to perform detailed diagnostics to fully characterize the H/NF_2 reaction. Species that were measured included $N_2(A)$, $N_2(B)$, $N_2(C)$, $NF(b)$ and $NF(a)$. Other parameters that were measured included the flows of the input reagents, the combustor and cavity pressure, the heat loss in the combustor and the cavity temperature. An additional diagnostic tool was video monitoring of the tests to provide a record of the changes occurring in the system as various parameters were changed. These measurements provided a detailed picture of processes occurring in the device.

This report is arranged as follows. The experimental apparatus and diagnostics are described in detail in Section 2. The experimental results are presented in Section 3. A discussion of the results is presented in Section 4. Finally, conclusions of the study are summarized in Section 5.

2. EXPERIMENTAL

2.1 EXPERIMENTAL APPARATUS

The experimental device consisted of an HF supersonic diffusion mixing laser with a gain length of 2.5 cm. The device used a HYLITE mixing nozzle that allowed addition of reactants at several distances downstream from the nozzle throat, allowing staged injection of reactants. This staging was used to allow versatility in the point at which reagents were introduced into the flow and to allow optimization of $N_2(A)$ production. A schematic diagram of the overall system is shown in Figure 1. The laser is constructed in a modular block arrangement.

2.1.1 Combustor

The combustor is a water-cooled nickel housing with an inside square cross section of 2.5 cm. It is closed at one end by a standard $F_2/H_2/He$ burner. The exit of the combustor contains an 18:1 expansion ratio supersonic nozzle with a 0.08 cm throat width. A photograph of the combustor is shown in Figure 2.

2.1.2 Mixing Nozzle

The primary mixing nozzle was developed under the Hypersonic Wedge Nozzle Concepts program and is a variation of the HYLITE nozzle. A photograph of one half of the nozzle is shown in Figure 3. It consists of six rows of injection holes. Reactants are injected through adjacent pairs of holes, giving three separate injection ports. The placement of the injector in the cavity and the positions in which reactants were injected are illustrated in Figure 1.

2.1.3 Laser Cavity

The combustor/nozzle assembly is attached to a rectangular aluminum cavity with a square cross section of approximately 12 cm on a side. It

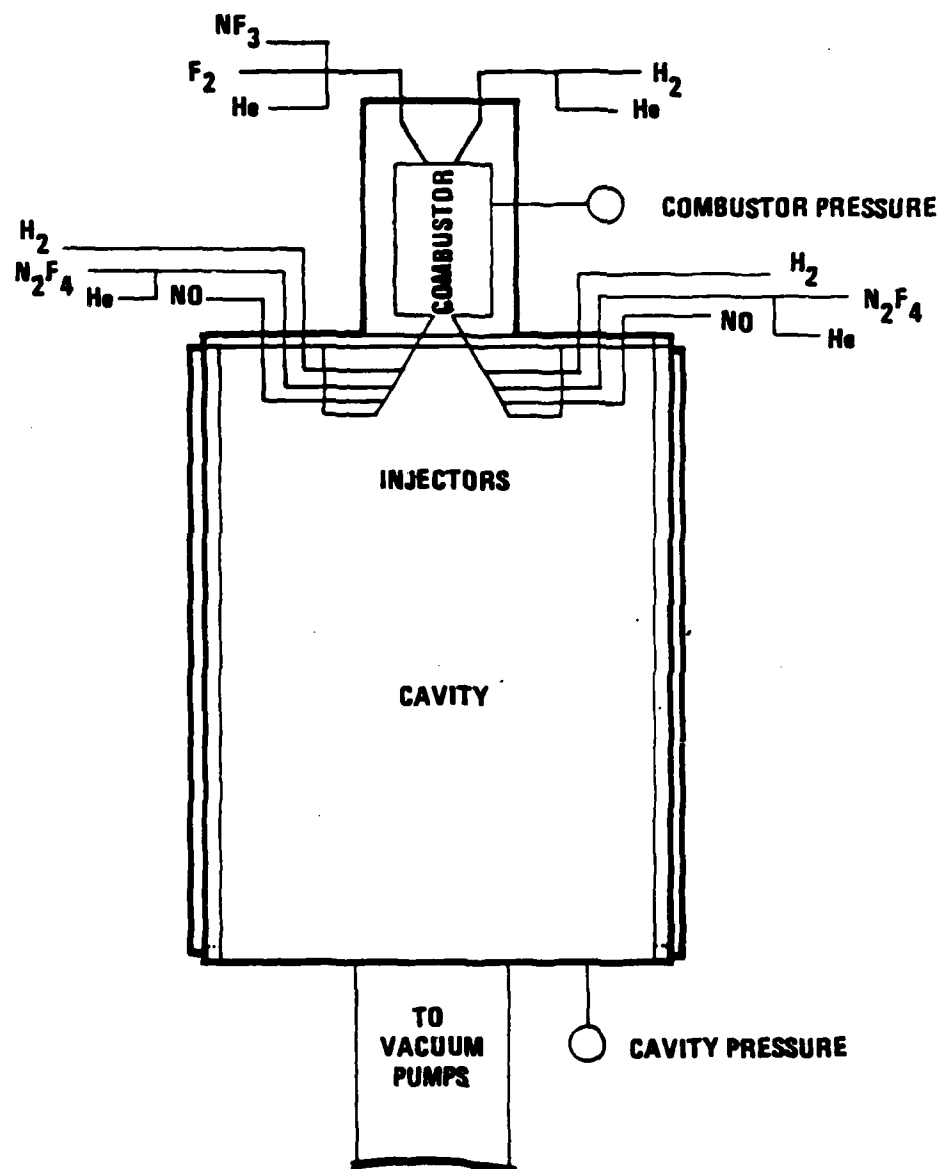


Figure 1. Schematic diagram of system used to study scaling of excited nitrogen production.

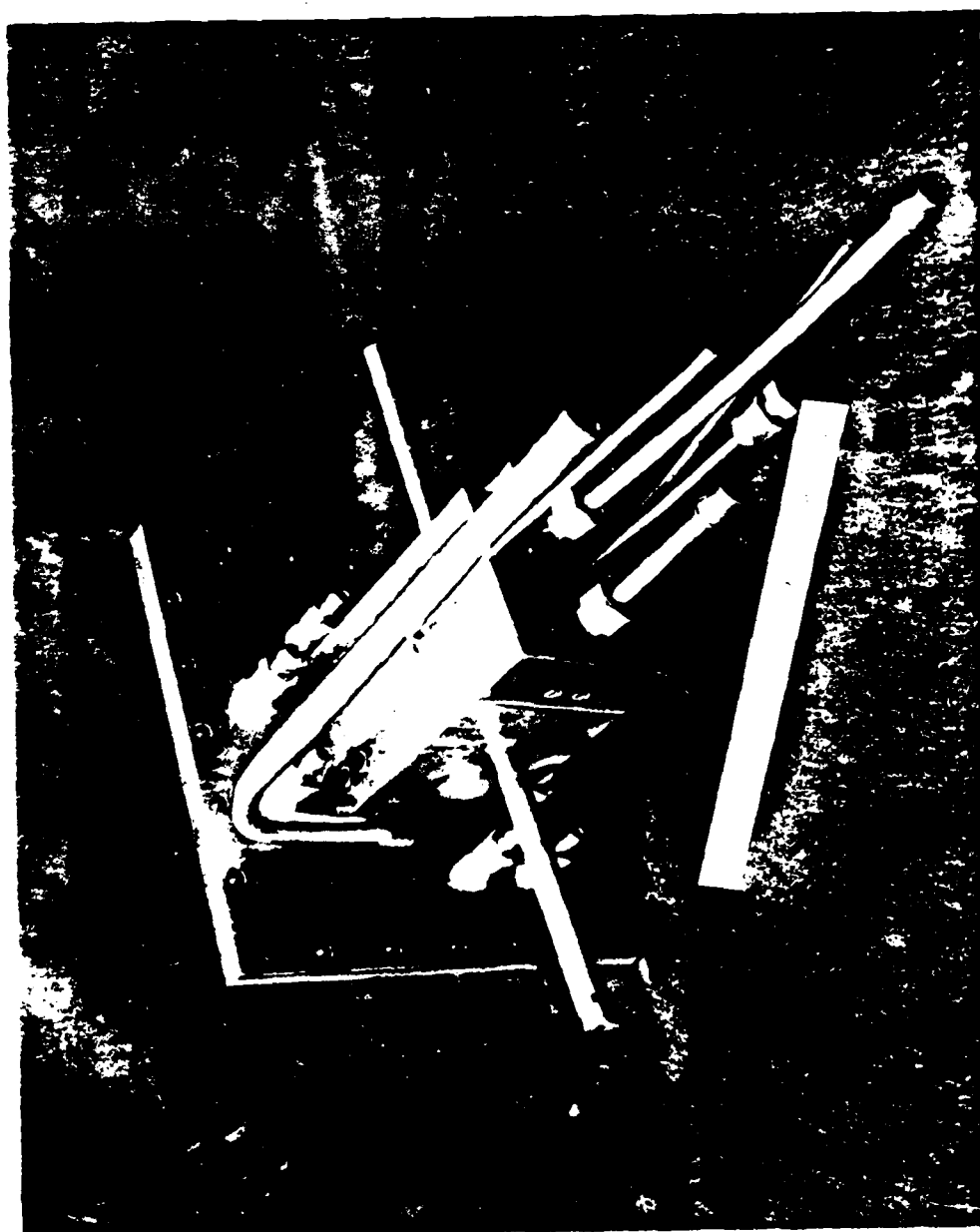


Figure 2. Photograph of combustor used to produce F-atoms.

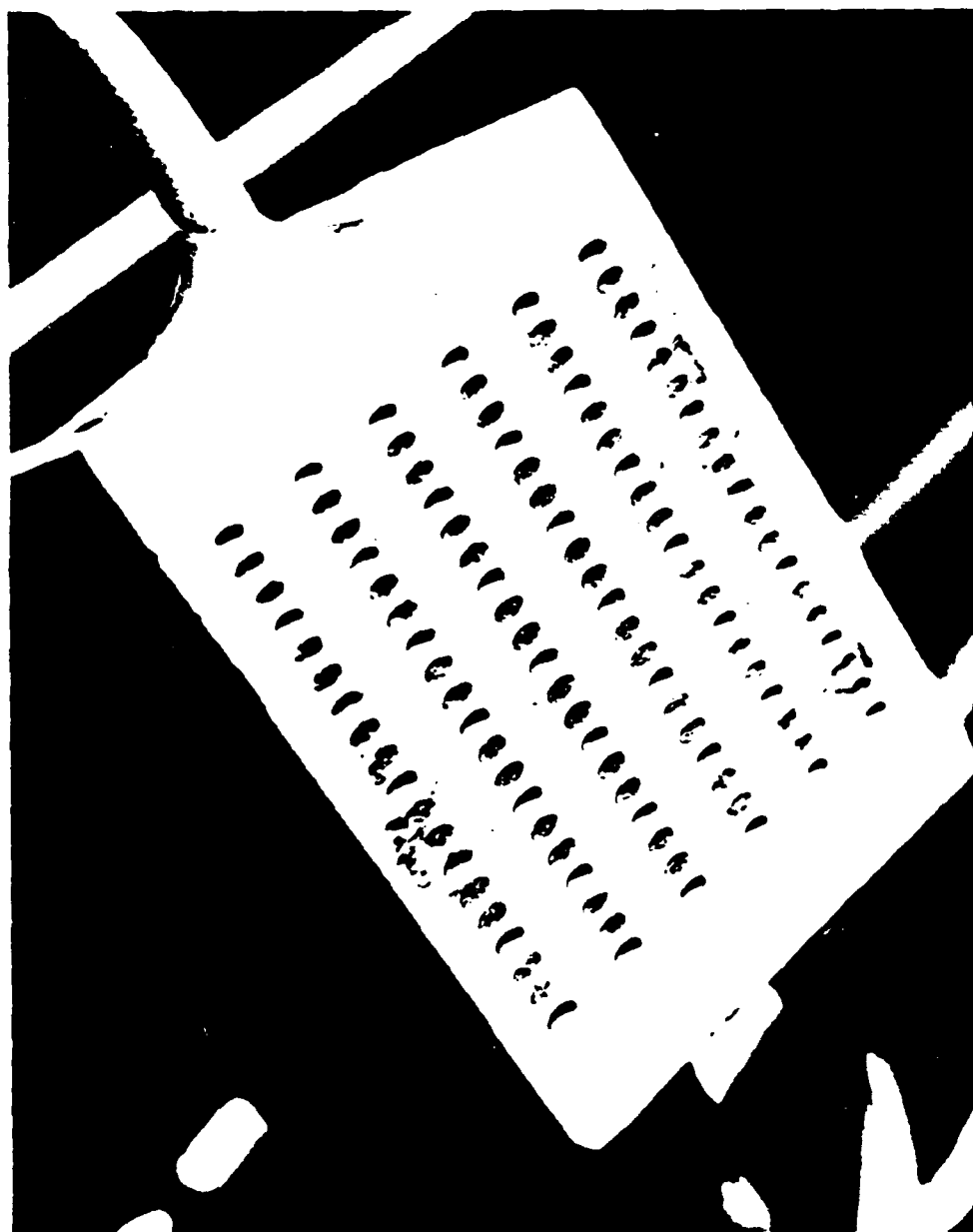


Figure 3. One section of HYLYTE nozzle used to mix H_2 and NF_2 with F-atom flow.

has four fused silica windows, approximately 15 cm long and 5 cm wide, to allow for diagnostic measurements. A photograph of the cavity with combustor attached is shown in Figure 4. The viewing distance for diagnostics was referenced to the bottom of the HYLITE nozzle. This distance is referred to as X_c .

2.2 GAS DELIVERY SYSTEM

The reactant gases are all metered to the device by critical flow orifices contained in a flow control panel. As long as the pressure drop across the orifice is greater than 2, sonic flow is established through the orifice and gas flow is linearly proportional to upstream gas pressure. The orifices were initially calibrated with reference to a Matheson linear mass flow transducer. However, some discrepancies were noted in these calibrations and, consequently, the calibrations were repeated by flowing the gas into a known volume. The pressure rise associated with a measured time of flow results in a direct measurement of the flow rate. The calibrations were performed with the actual gases, i.e., H_2 , F_2 , He, and NF_3 .

All reagent gases were used without further purification. However, the presence of NO emission in flames with only H_2 , F_2 and N_2F_4 led to the question of N_2F_4 purity. Consequently, a sample from each of the N_2F_4 bottles was sent to Hercules Incorporated, Magna, Utah, for analysis with a gas chromatograph. A summary of the analysis is shown in Table 1 and a plot of the peaks in the gas chromatograph is shown in Figure 5. Note that there is a substantial amount of NO and N_2O in all N_2F_4 samples which can accept energy from the $N_2(A)$ and radiate. There is also a large unidentified peak indicating the presence of some unknown impurity.

2.3 OPTICAL DIAGNOSTICS

The optical diagnostics associated with these experiments collected emission in both the infrared and visible spectral regions. The diagnostics are summarized in Table 2. A photograph of the device with

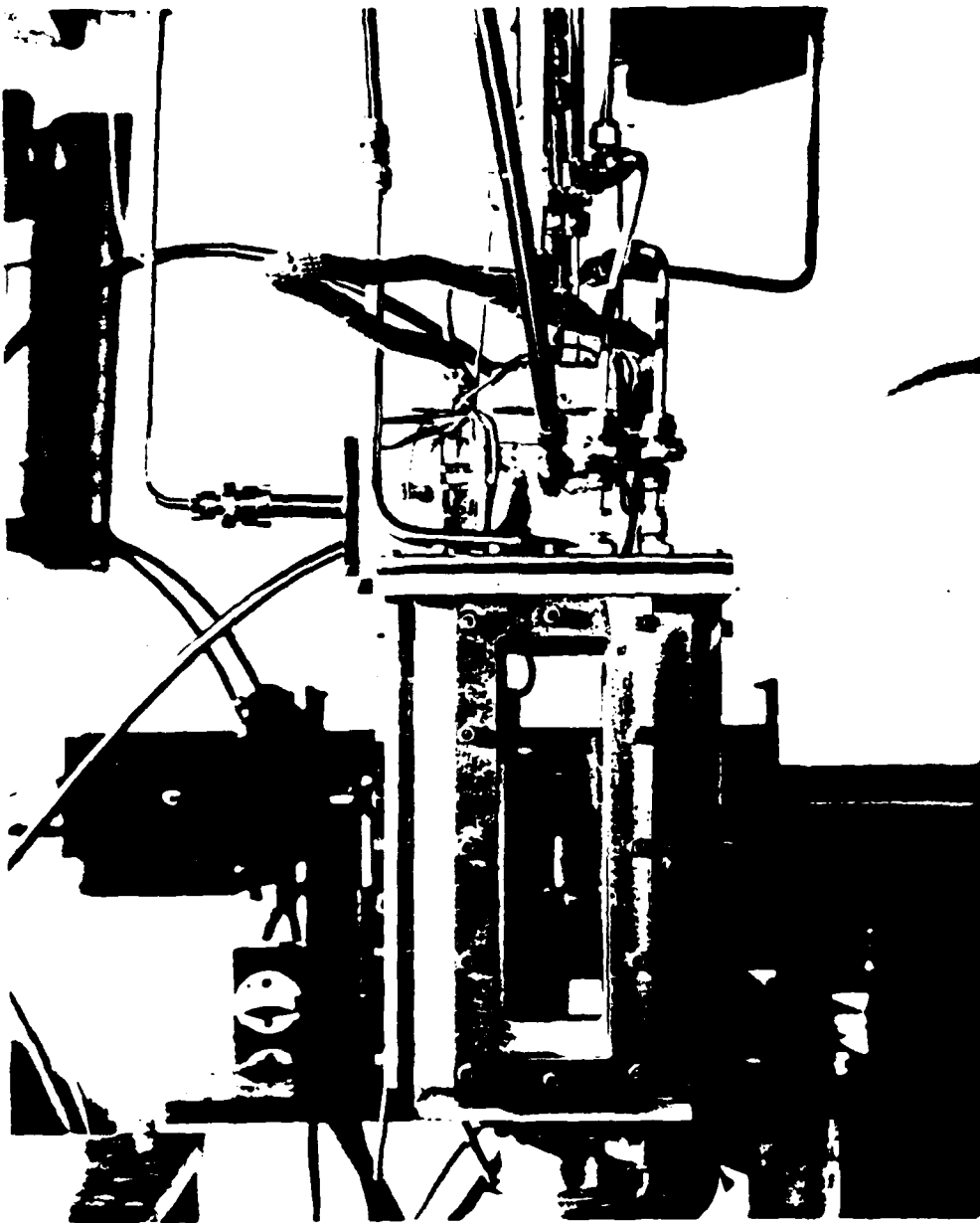


Figure 4. Assembled device showing laser cavity.

TABLE 1. ANALYSIS OF GFE FURNISHED N_2F_4

SPECIES	PERCENT COMPOSITION				
	1977 VINTAGE	12	13	14	15
N_2	9.1	4.9	4.8	5.4	4.9
CO	ND (<0.05)	0.24	1.33	0.0007	0.07
NO	ND (<0.05)	0.15	0.29	0.41	0.18
CF_4	ND (<0.05)	-	-	-	-
NF_3	0.14	-	-	-	-
N_2F_2	0.13	-	-	-	-
CO_2	ND (<0.05)	0.052	0.11	0.04	0.04
N_2O	0.25	0.34	0.38	0.29	0.41
N_2F_4	90.4	-	-	-	-
Unknown 1 ^a	-	0.94	0.96	1.2	0.99
Unknown 2	-	3.4	3.9	3.9	3.6

^a The retention time of Unknown 1 is similar to that of NF_3 but not identical.

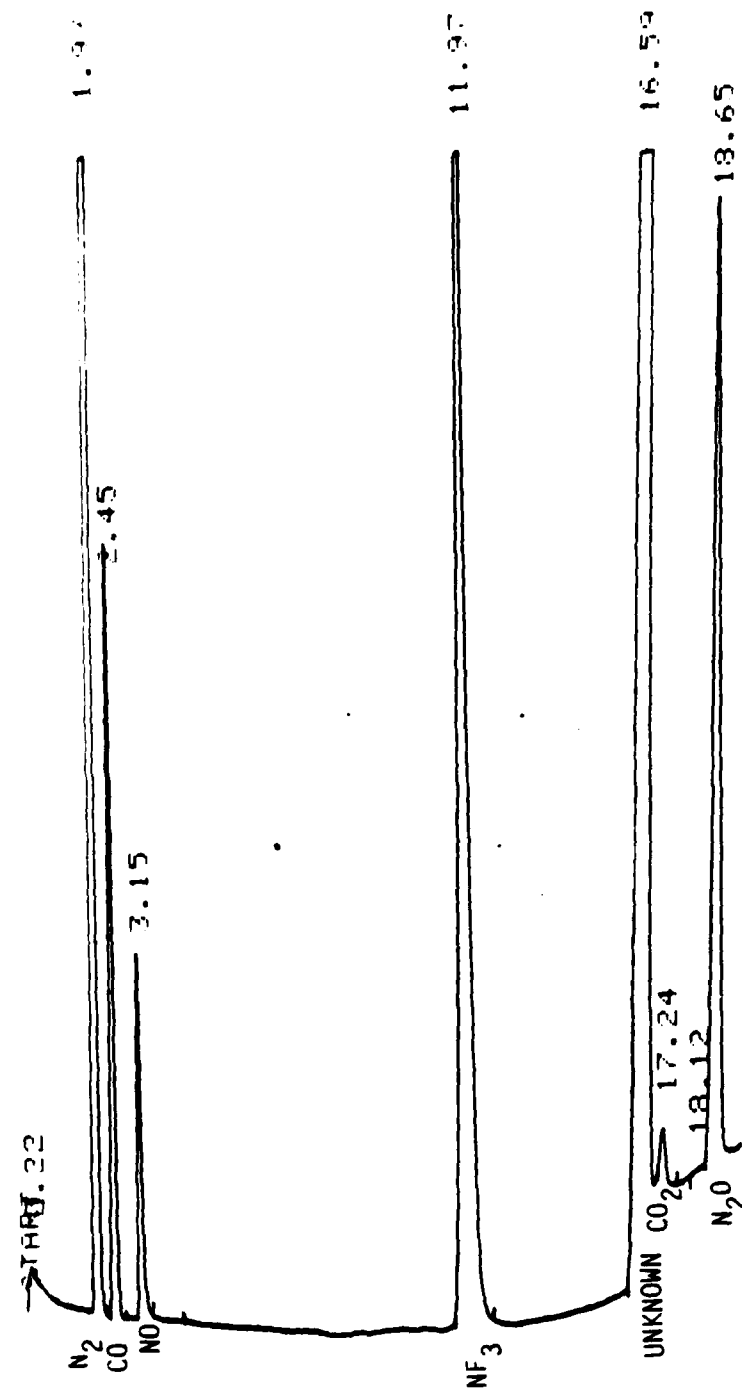


Figure 5. Peaks in gas chromatograph analysis of N_2F_4 provided by Hercules.

TABLE 2. SUMMARY OF DIAGNOSTICS USED TO CHARACTERIZE EXPERIMENTS

SPECIES	TECHNIQUE	ERROR ^a SOURCES	ESTIMATED ERROR
N ₂ (B)	VISIBLE EMISSION SPECTROSCOPY	UNOBSERVED INFRARED EMISSION	± 20%
NF(b)	VISIBLE EMISSION SPECTROSCOPY	BASELINE	± 10%
N ₂ (C)	ULTRAVIOLET EMISSION SPECTROSCOPY	MASKED EMISSION BASELINE	± 100% ± 100%
N ₂ (A)	INFER FROM N ₂ (C); TITRATION WITH NO, CO	INDIRECT DETERMINATION	ORDER OF MAGNITUDE
TEMPERATURE	HF CHEMILUMINESCENCE	ROTATIONAL NONEQUILIBRIUM SELF-ABSORPTION	± 20%
FLOW RATES	PRESSURES BEHIND CALIBRATED ORIFICES	STATISTICAL	< ± 10%
PRESSURES	CALIBRATED TRANSDUCERS	STATISTICAL	< ± 10%

^a ALL ABSOLUTE EMISSION MEASUREMENTS HAVE ± 30% RADIOMETRIC UNCERTAINTY

diagnostics attached is shown in Figure 6. The Tracor Northern Intensified Diode Array Spectrometer is shown on the right of the picture with its associated collection optics, spectrometer and detection head behind the optical cavity. The infrared spectrometer with collection optics and detector is to the left of the picture in front of the cavity. A schematic diagram of the device with its attached diagnostics is shown in Figure 7.

The Tracor Northern Intensified Diode Array Spectrometer was chosen for this study because it permits parallel accumulation of a large spectral region, thus preventing instrumental distortions that can be introduced into recorded spectra by conventional scanning spectrometers. An ungated, ultraviolet (UV) intensified head was chosen at the beginning of the program when the most critical issue was determined to be sufficient detector sensitivity to record $N_2(A)$ emission directly. As testing progressed, it was discovered that the $N_2(A)$ emission was masked by $NO(A-X)$ emission, making direct detection of $N_2(A)$ impossible. The sensitivity of the UV intensified head falls dramatically at wavelengths greater than about 650 nm, making the detection of spectral features at these longer wavelengths much more difficult. Obtaining an additional unintensified head was not an option at this point of the program.

The Tracor Northern detector head was connected to a Spex 0.25 m f/4 flat field spectrograph to resolve the spectrum. A selection of holographic gratings blazed at 300 nm, 500 nm, and 750 nm was available to provide variable coverage and resolution over the spectral response of the detector, while minimizing internal scattered light and eliminating grating ghosts. Care was taken to assure detector-spectrograph focal plane alignment for maximum spectral resolution with any given grating. Additionally field flatness, spectrograph vignetting, and detector spatial sensitivity were measured with a diffuse narrow line source to maximize system performance.

For some tests a 0.3 m McPherson monochromator equipped with an Hamamatsu R763 photomultiplier tube was used to record emission spectra.

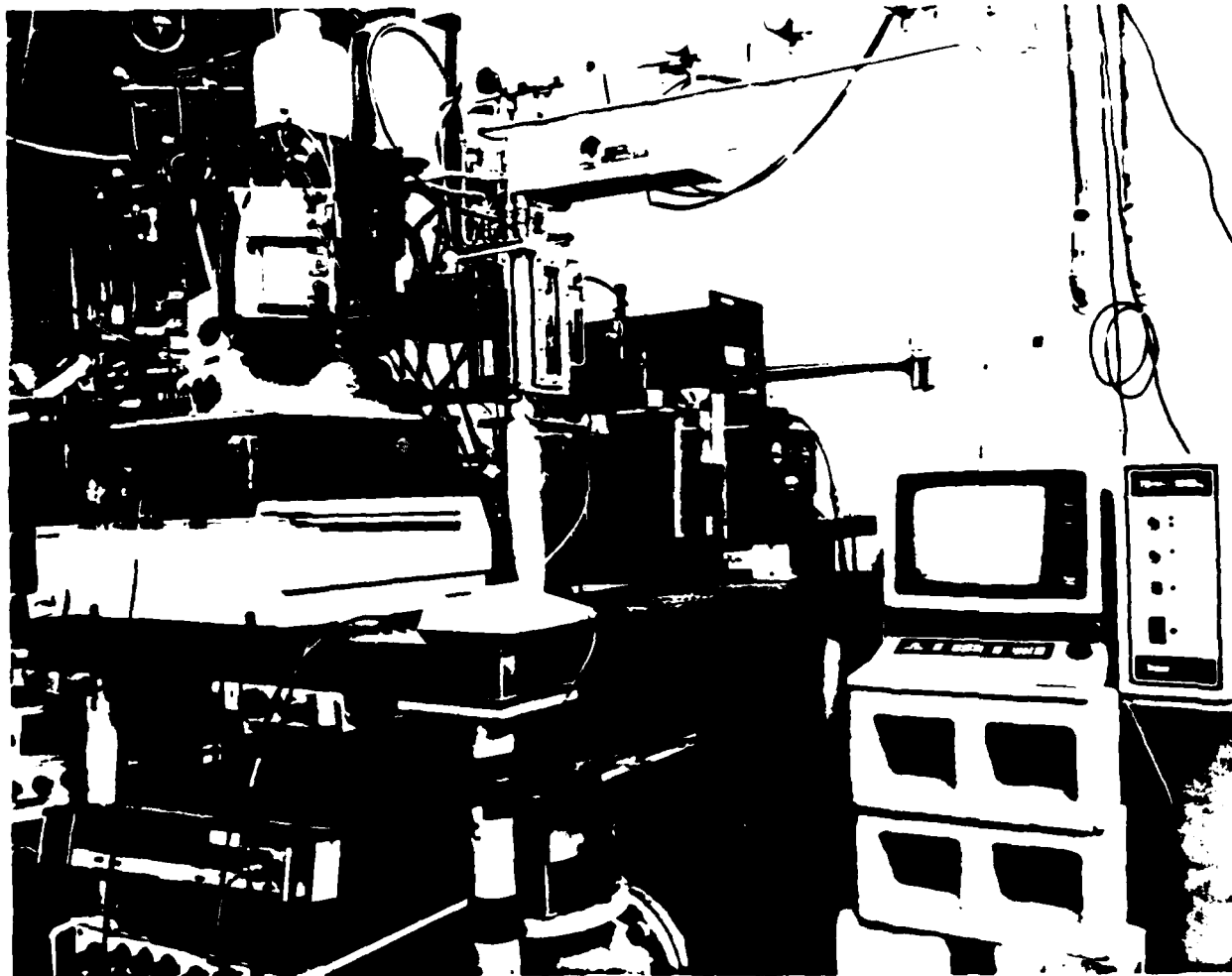


Figure 6. Photograph of device with attached diagnostics

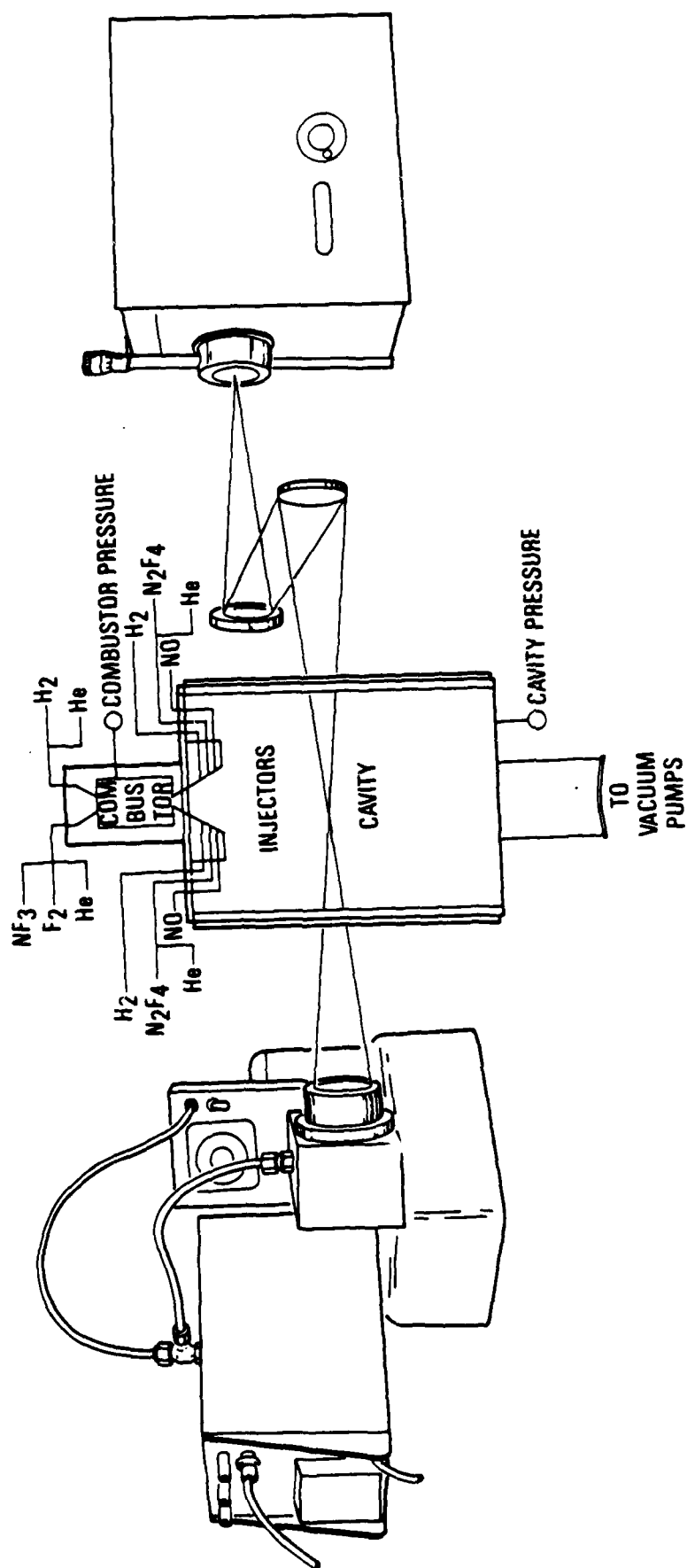


Figure 7. Schematic of device showing arrangement of diagnostics

This spectrometer allowed accumulation of higher resolution spectra than could be obtained with the Diode Array Spectrometer and was used for spectral identification and some careful calibration comparisons. Both the slit function and the phototube gain and linearity versus anode-cathode voltage were characterized on this system. Spectrometer scan rates were chosen to account for the measured recorder slew rates in an effort to minimize instrumental integration.

The light from the diffuse reaction volume was collected by 1:1 imaging optics as shown in Figure 7. A tenth wave, 4.6-cm-dia 0.3-m spherical mirror and a single twentieth wave MgF_2 overcoated flat mirror were arranged to collect light from the central flow volume (see Fig. 8). A 1:1 image transfer was accomplished by placing the spherical mirror at the radius of curvature distance from the center of the flow volume under investigation. If the angle θ is kept less than 10 deg, then the off-axis imaging performance of the spherical mirror is not appreciably degraded by tangential/sagittal astigmatism. The use of reflective (versus refractive) collection optics eliminates most chromatic aberration usually associated with the imaging of a broadband source and hence, an acceptable 1:1 image transfer to the spectrograph slit results. Location of the viewing volume in the supersonic flow was determined by the use of a HeNe laser to align the collection optics with the spectrograph optical axis. The viewed volume was the volume defined by the translation of the slit area (with cross section dimensions determined by the slit width multiplied by the detector active area height) along the line of sight (Fig. 9) between the flow boundaries. This volume is labeled collection volume in Figure 9. Although the volume bounded by the collection cones and flow boundaries is significantly larger than the collection volume, the light collection efficiency from planes parallel to the slit image plane within the collection cone volume (e.g. plane A) falls off as $1/R^2$, while the cross sectional area of plane A increases as R^2 . The net effect is to produce an equivalent viewing volume with dimensions of the shaded collection volume of Figure 9. An experimental verification of the line of sight ($1/R^2$, R^2) effect was performed using a HeNe laser and translatable Lambertian diffuser plate as a diffuse source, and a spherical mirror as the collection optic (Fig. 10). If the HeNe laser

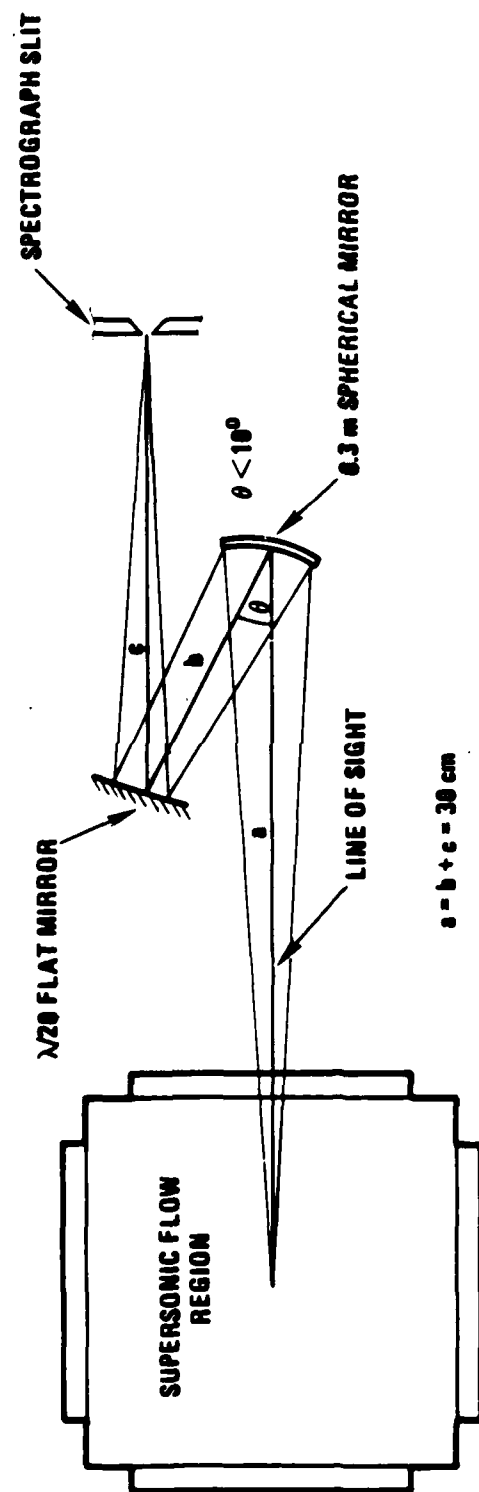


Figure 8. Optical layout for diagnostics

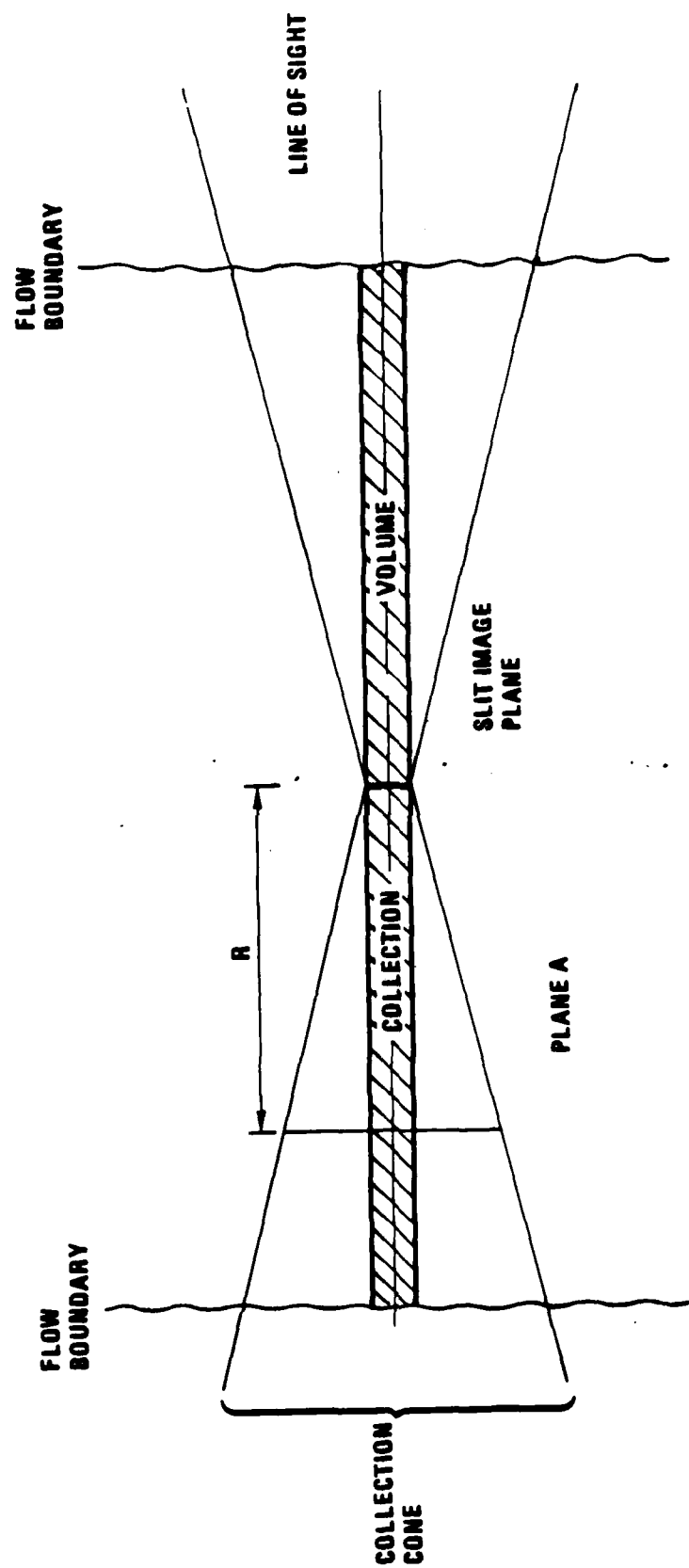


Figure 9. Collection Optics

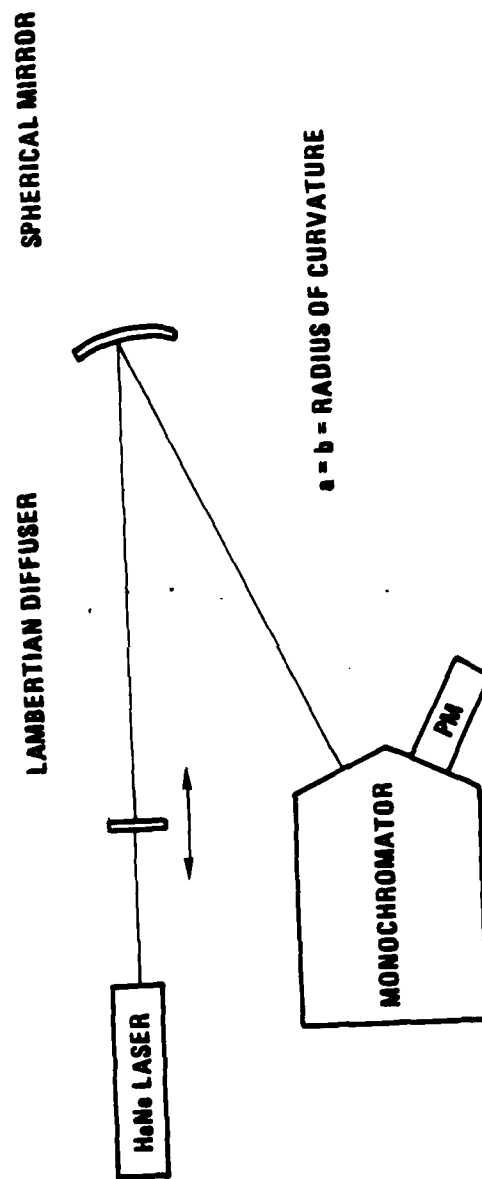


Figure 10. Experimental layout to verify line of sight effect.

beam axis is aligned coaxially with the monochromator/spherical mirror optical axis, it can be demonstrated that the translation of the diffuser plate has no effect on the signal level collected at the output slit.

One source of uncertainty in the absolute radiometric calibrations is the flow boundary separation distance. Because the supersonic flow is allowed to freely expand, the flow boundaries along the line of sight are not well defined and introduce uncertainty in the value assigned to the collection volume. This error has been conservatively estimated at +10% since the visible emission clearly demarcates the flow boundary. A potentially greater source of error exists in the choice of radiance standards used to calibrate the 250-nm to 400-nm spectral region. While standard Eppley lamps and blackbody sources are readily available and their outputs calibrated in the near UV, their visible/UV output ratio is typically so large that in all but the highest rejection ratio spectrographs, the internal scattered light from the visible region seriously interferes with near UV radiometric accuracy. Any selective filtering of the output from the standards necessarily alters the radiance or irradiance values and, thus, a region-specific source should be used. For this purpose, a radiance and irradiance calibrated deuterium standard lamp was used due to its selective near UV output. A constant temperature, variable irradiance source could be generated through the $1/R^2$ irradiance dependence; similarly, variable radiance values were obtainable if an NBS calibrated Teflon diffuser disc was irradiated at carefully measured distances.

A separate near UV calibration of the spectrograph and collection optics was carried out to independently test optical component performance. The spectrograph-detector head sensitivity was first tested with the deuterium irradiance standard illuminating the input slit. The overall calculated sensitivity closely agreed with published values of detector response, grating efficiency, and spectrograph throughput. A UV radiance measurement was then performed utilizing both the collection optics and spectrograph for the final sensitivity values.

Detection sensitivity in the visible and near infrared (IR) regions was measured with Eppley and blackbody radiance standards for all intensifier gain settings and gratings used in the visible and IR radiance measurements. Good reproducibility was obtained with these two independent standards.

2.3.1 $N_2(A)$ Diagnostic

The original program plan was to observe $N_2(A \rightarrow X)$ emission directly. However, it was found that the NO impurity in the N_2F_4 supply caused the $N_2(A \rightarrow X)$ spectrum to be obscured by $NO(A \rightarrow X)$ emission. Several high resolution spectra like that in Figure 11 were taken to try to resolve the $N_2(A \rightarrow X)$ spectrum from the $NO(A \rightarrow X)$ spectrum. Under no condition could the $N_2(A \rightarrow X)$ spectrum be observed. Upper limit estimates could be made based on the fact that it was not observed that show it was less than 10^{12} molecules/cm³. To get a better estimate, the $N_2(A)$ was estimated from the $N_2(C)$ density (see description of $N_2(C)$ diagnostic), making the assumption that the $N_2(C)$ is formed by the pooling reaction between two $N_2(A)$ molecules as shown in Equation 5. With this assumption, the $N_2(A)$ density can be expressed as

$$[N_2(A)] = \sqrt{[N_2(C)]/k_5 \cdot \tau_C} \quad (9)$$

where $k_5 = 2.6 \times 10^{-10}$ cm³ molecule⁻¹ s⁻¹ and τ_C is the radiative lifetime of $N_2(C)$, 1.0×10^{-8} s⁻¹.

An attempt was made to titrate $N_2(A)$ with NO, using the $NO(A \rightarrow X)$ emission as a diagnostic. However, this approach proved to be inconclusive because of the difficulty in uniformly mixing the NO into the active stream and the absence of a sharp endpoint. This is discussed further in Section 3.

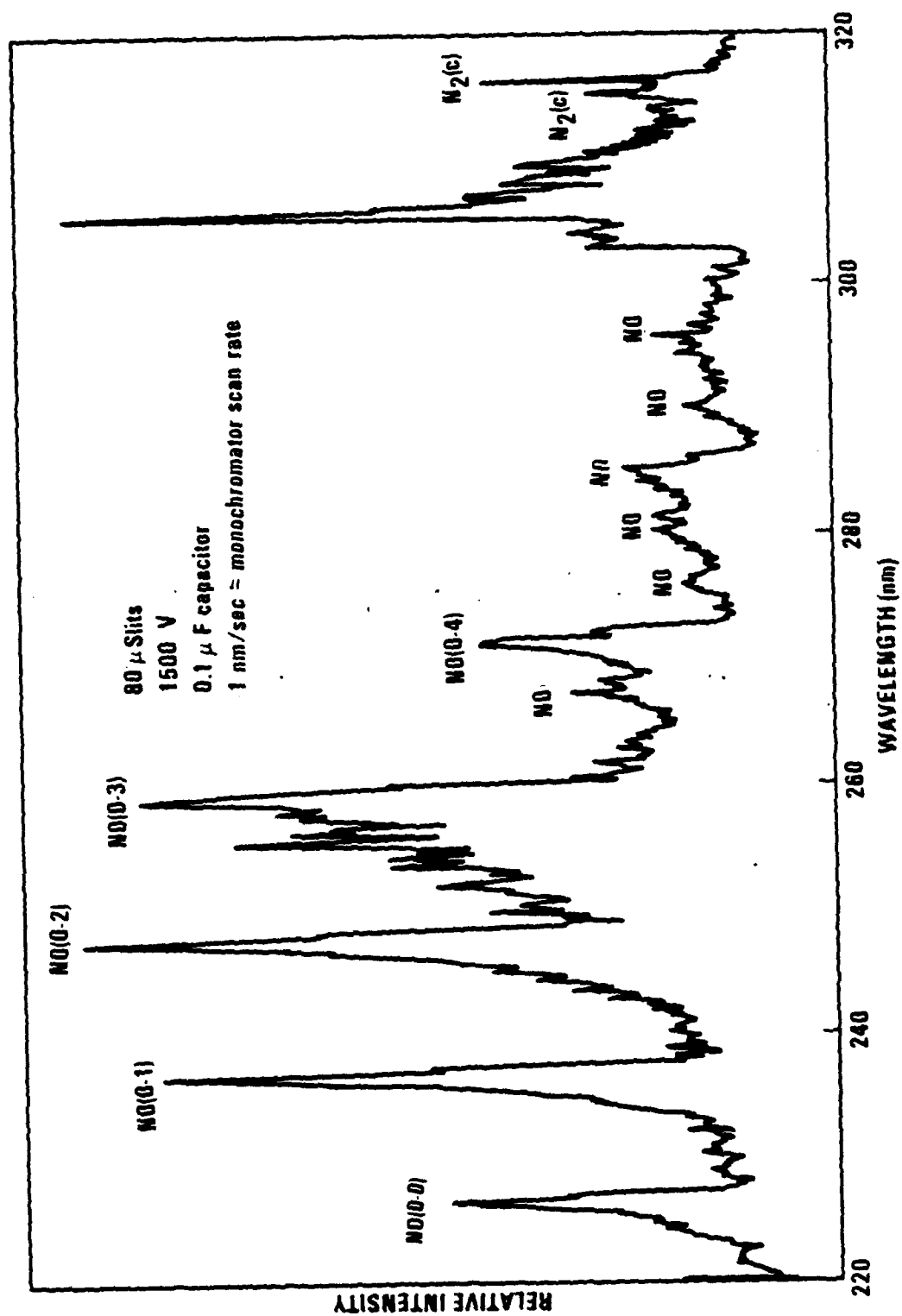


Figure 11. High resolution UV emission spectrum.

2.3.2 N₂(B) Diagnostic

Emission from the N₂(B→A) transition in the 520 to 800 nm spectral region was recorded with the Tracor Northern Diode Array Spectrometer calibrated against a standard radiance lamp and a blackbody standard. Total density in the B state is obtained by integrating the area under the observed chemiluminescent spectrum and applying a correction factor for emission in the wavelength region longer than 800 nm which was not recorded by the Intensified Diode Array Spectrometer. This correction factor was directly obtained by measuring the 800 to 1100 nm emission with a 0.3 m McPherson spectrometer equipped with a cooled germanium detector.

2.3.3 N₂(C) Diagnostic

Observation of the emission from the H/NF₂ reaction system indicated that part of the N₂(C→B) spectrum was obscured by emission from the NH(A→X) spectrum and other unidentified emissions. The lines that were resolvable are a $\Delta v = -1$ sequence of lines at 315.9 nm, 313.6 nm, and 311.6 nm, the $v' = 1 \rightarrow v'' = 2$ line at 353.7 nm and the $v' = 0 \rightarrow v'' = 1$ line at 357.7 nm. A line at 380.5 nm due to the $v' = 0 \rightarrow v'' = 2$ transition could be observed but not totally resolved from the other structure. In addition, there was a large line at 375.5 nm where the $v' = 1 \rightarrow v'' = 3$ line occurs. However, this line did not follow the published intensity distributions expected for N₂(C) lines. It was believed that this line probably came from some other system. If the intensity of the line at 375.5 nm was used in estimating N₂(C), it would up the N₂(C) density estimates in this report by approximately a factor of 10. Because the large NH peak saturated the spectrum analyzer when it was centered at this wavelength, it was convenient to use features on either side of the NH line to diagnose N₂(C). It was finally decided to use the 353.7 nm and 347.7 nm lines. The absolute number of photons in these two lines was obtained by measuring the area under the spectral curves. The absolute number of photons in the the $v' = 1$ level of the C state was obtained from

$$N(v' = 1) = I(v' = 1 \rightarrow v'' = 2) \tau_A / FCF (v' = 1 \rightarrow v'' = 2)$$

where $I(v' = 1 \rightarrow v'' = 2)$ is the number of photons/cm³ s in the 353.7 nm band, τ_C is the radiative lifetime of the C state, and $FCF(v' = 1 \rightarrow v'' = 2)$ is the Franck-Condon factor for the $v' = 1$ to $v'' = 2$ transition, .212. A similar formula was used to obtain the population in the $v' = 0$ state from the radiation in the 357.7 nm band. The relative populations in the $v' = 1, 2$ and 3 states was obtained from the relative intensities of the lines at 315.9(1-0), 313.6(2-1) and 311.7(3-2) nm with their respective Frank-Condon factors. The total correction factor is approximately 10. The Tracor Northern Diode Array Spectrometer was calibrated in the UV region with a deuterium radiance standard was used for this measurement.

2.3.4 NF(b) Diagnostic

The NF(b \rightarrow X) emission spectrum at 528.8 nm was easily separated from the N₂(B \rightarrow A) emission. The NF(b) density was determined from the intensity of this emission peak and the radiative lifetime of NF(b).

2.3.5 NF(a) Diagnostic

For all the conditions run in the experiments where an attempt was made to optimize the N₂(B) emission, the NF(a \rightarrow X) emission spectrum at 892 nm is overlapped by the N₂ first positive emission spectrum and HF vibrational overtone emission. This is shown clearly in Figure 12 which is a representative spectrum for the device. If flows were adjusted to make the flame appear green rather than yellow; i.e. maximizing NF(b) rather than N₂(B), then the NF(a \rightarrow X) spectrum could be resolved but the N₂(A) was not optimum. This problem was encountered earlier (Ref. 5) where N₂(A) could not be resolved from NF(a) emissions. Finally, NO was added to the system to remove N²(D) atoms which are the precursor of the N₂(B) so NF(a) could be measured with no N₂(B) emission. The same problem was encountered as described in Reference 6. A high resolution spectrum was combined with a computerized synthetic spectrum analysis to separate the nitrogen and HF emissions from NF(a). Isolation of NF(a) emission would require even higher resolution than achievable with the .03 m McPherson spectrometer used to

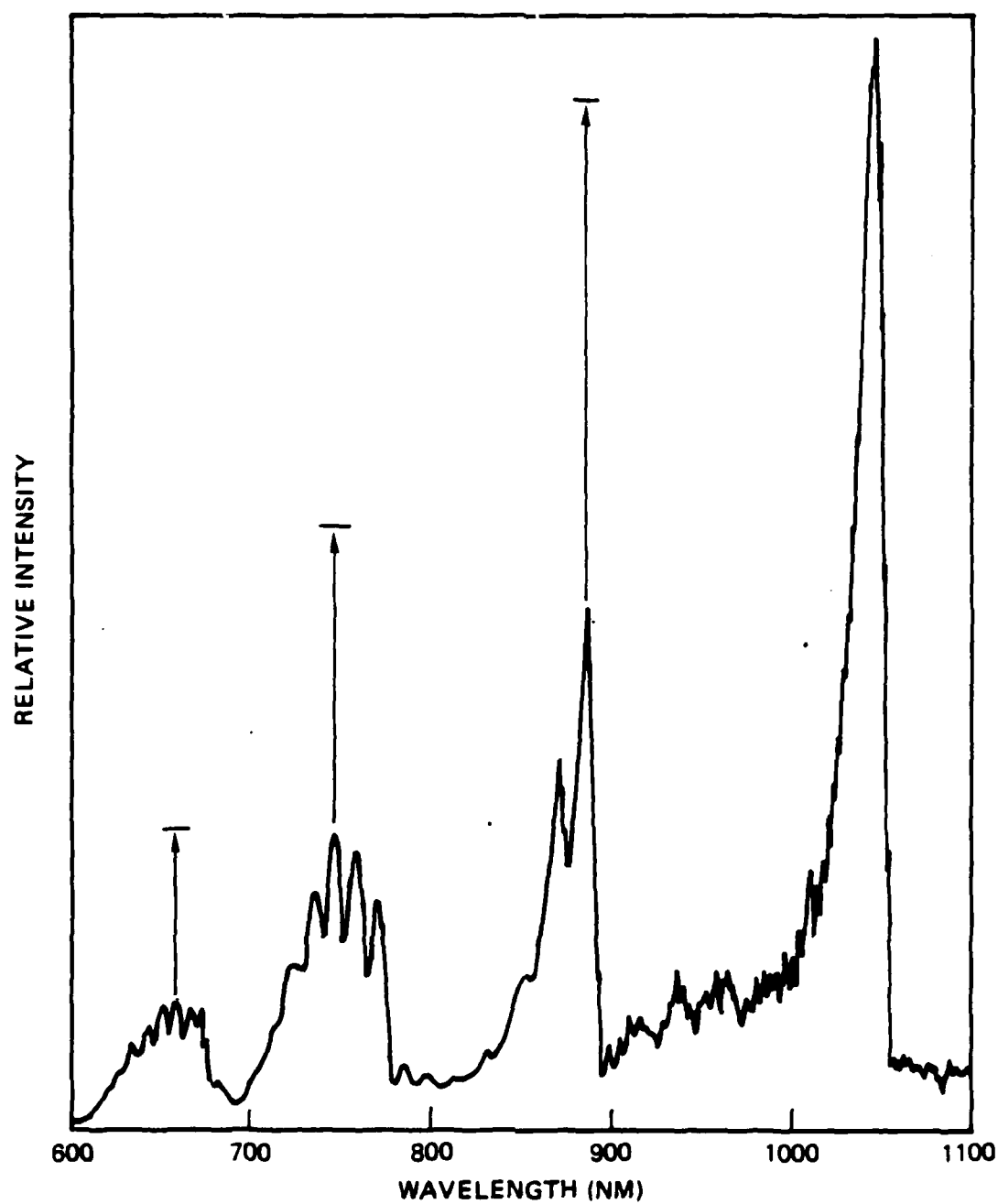


Figure 12. Spectrum from 600 to 1100 nm. Arrows show correction for spectral response of detector.

obtain the spectrum shown in Figure 12. This became too complicated to do in these experiments where the primary goal was to optimize N_2 emissions rather than NF emissions. Hence, only upper estimates could be made based on the background emission.

2.3.6 Temperature Diagnostic

The cavity temperature was measured using HF IR chemiluminescent spectroscopy. A 0.3 m McPherson Spectrometer with a 150 line/mm, 4 μ m blaze grating was used with a liquid nitrogen cooled, InSb photovoltaic detector. A chopper and lock-in amplifier were used for phase sensitive detection. The entire optical path and spectrometer were flushed with dry nitrogen to remove atmospheric water vapor which interferes with the HF spectrum. The optical system was calibrated with a blackbody source to correct the detection system for sensitivity variations as a function of wavelength.

The peak intensities of the HF lines were hand read and input into a computer code that constructed Boltzmann plots to compute the rotational temperature. The HF(1 \rightarrow 0) emission data were usually nonlinear due to self absorption from HF(0 \rightarrow 1) and were not used.

2.4 TEST PROCEDURE

Diagnostics used in the tests were discussed in the previous section. However, during a series of test runs, some criteria had to be established to quickly evaluate the value of the test in question. Because $N_2(A)$ emission could not be observed directly and much of the $N_2(C)$ emission was obscured by NH peaks, it was decided that the intensity of the $N_2(B\rightarrow A)$ emission was a good figure of merit for evaluating the performance of the device. Observing the $N_2(B\rightarrow A)$ emission with the Tracor Northern Diode Array Spectrometer in real time made this task relatively simple. Studies were made that verified that most other emissions observable in the system tracked the $N_2(B\rightarrow A)$ intensity, justifying this procedure. In a normal test series, an X_c position was first chosen, then flows were varied with the $N_2(B\rightarrow A)$ spectrum being

recorded for each set of flows. A new X_c was then chosen and the optimization repeated. After a series of runs, the recorded set of spectra were reviewed and detailed diagnostics performed only on the optimum test series. The detailed diagnostics included a scan of all emission intensities versus X_c .

3. RESULTS

3.1 SPECTROSCOPY

Spectra were taken over the region from 220 to 1100 nm. The spectrum from 220 to 320 nm was shown in Figure 11. Note that almost all the peaks could be assigned to NO(A \rightarrow X) emission. The radiative lifetime of the NO(A) state is 200 ns (Ref. 7) whereas the radiative lifetime of N₂(A) is 2 s (Ref. 8). The difference of 1×10^7 in radiative lifetime indicates that relatively small amounts of NO could mask the N₂(A) emission. The analysis of N₂F₄ presented in Table 1 showed the NO to be approximately 0.3 per- cent of the N₂F₄. If even a fraction of this NO is converted to NO(A), the resulting A \rightarrow X emission could effectively mask any N₂(A \rightarrow X) emission. The spectrum from 320 to 350 nm is shown in Figure 13. This emission is on a scale that is a factor of 100 times greater than the spectra in Figures 11 and 14. This emission, peaked at a wavelength of 336 nm and assigned to NH(A³ Π \rightarrow X³ Σ), is the strongest emission observed in the entire system. However, integration under the curve and use of the published radiative lifetime of NH(A-X) of 455 ns (Ref. 9) indicates that the NH(A) density is only on the order of 10^9 molecules/cm³.

The spectrum from 350 to 390 nm is shown in Figure 14. As discussed in more detail in paragraph 2.3.3, N₂(C) lines at 353.7 nm and 357.7 nm could be completely resolved. An N₂(C) line at 380.5 nm could be observed but not totally resolved from the other spectral features. The large spectral feature at 375.5 nm falls where the $v' = 1 \rightarrow v'' = 3$ line of the N₂(C) spectrum lies. However, this line does not follow the published intensity distributions expected for the N₂(C) lines and hence we are reluctant to assign it to the N₂(C) system without further confirmation. The rotational structure apparent in this figure is not characteristic of the N₂(C) spectrum and suggests an H-containing compound.

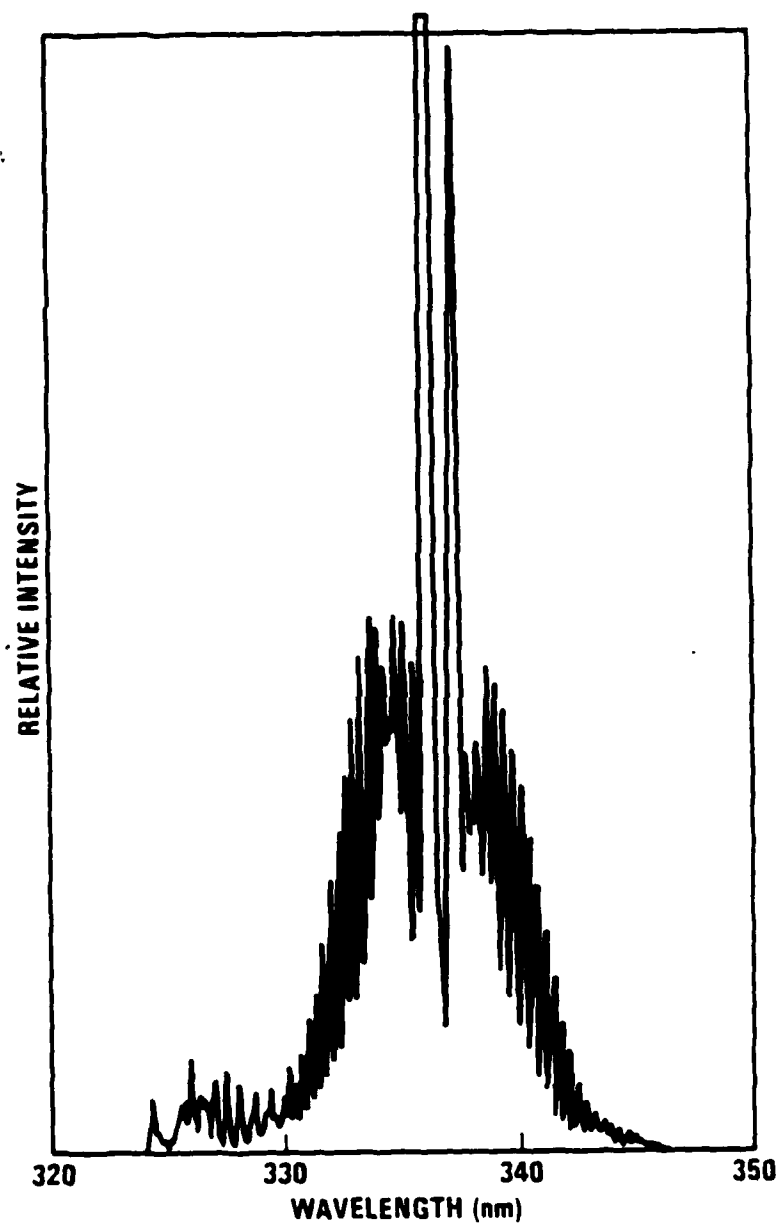


Figure 13. Ultraviolet emission spectrum from 320 to 350 nm showing NH(A-X) emission.

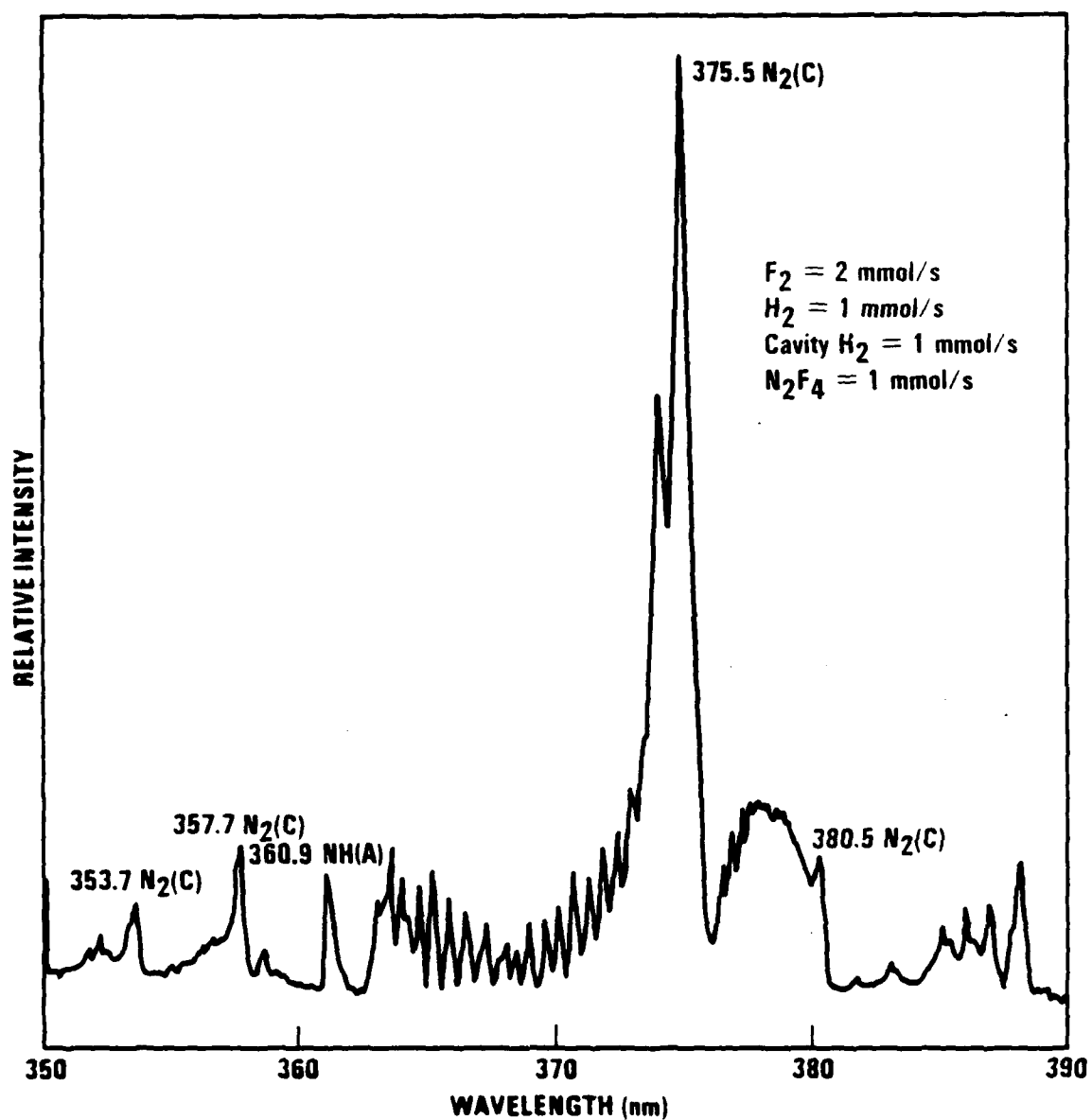


Figure 14. High resolution ultraviolet emission spectrum from 350 to 390 nm.

The spectrum from 500 to 800 nm is shown in Figure 15. This spectrum was taken with the Tracor Northern Diode Array Spectrometer and corrected for wavelength. The spectrum from 600 to 1100 nm was shown in Figure 12. These spectra show the total $N_2(B \rightarrow A)$ emission band. This spectrum is representative of all the runs made in the system. The $NF(b \rightarrow X)$ emission is seen in this scan at 529 nm. The $N_2(B)$ spectrum indicates that the $N_2(B)$ vibrational temperature is relatively cold since much of the intensity originates in the $v' = 0$ upper state. However, the region where $NF(a \rightarrow X)$ emission is to be expected is totally masked by the strong $N_2(B)$ emission. This differs from spectra that were obtained with the goal of enhancing $NF(a)$. It was difficult to obtain a pure $NF(a)$ spectrum with the hardware used in this experiment because of the strong interfering $N_2(B)$ peak.

3.2 DENSITY MEASUREMENTS

The experimental device was run in two modes. The nominal mode was to burn F_2 and H_2 in the combustor to produce F-atoms, to add H_2 through the first set of injection holes to produce H-atoms and then add heated N_2F_4 through either the second or third set of injectors to initiate the H/NF_2 chemistry. A variation of this mode was to inject NF_3 rather than N_2F_4 through the final set of injector holes. The second mode was to burn F_2 , H_2 and NF_3 in the precombustor to produce NF_2 radicals, F-atoms and HF, and then to add H_2 in the cavity to react with the F-atoms to produce H-atoms and hence initiate the H/NF_2 chemistry.

3.2.1 $F/H_2/N_2F_4$ Configuration

An extensive series of over 100 tests were run in this nominal configuration. In summary, it was found that there was little variation in $N_2(B)$ density when flows of combustor F_2 , combustor H_2 or cavity H_2 were varied. However, the emission intensity was directly proportional to the N_2F_4 (NF_2) flow. It was found that the $N_2(B)$ intensity was reproducible from day to day for a given set of flow conditions.

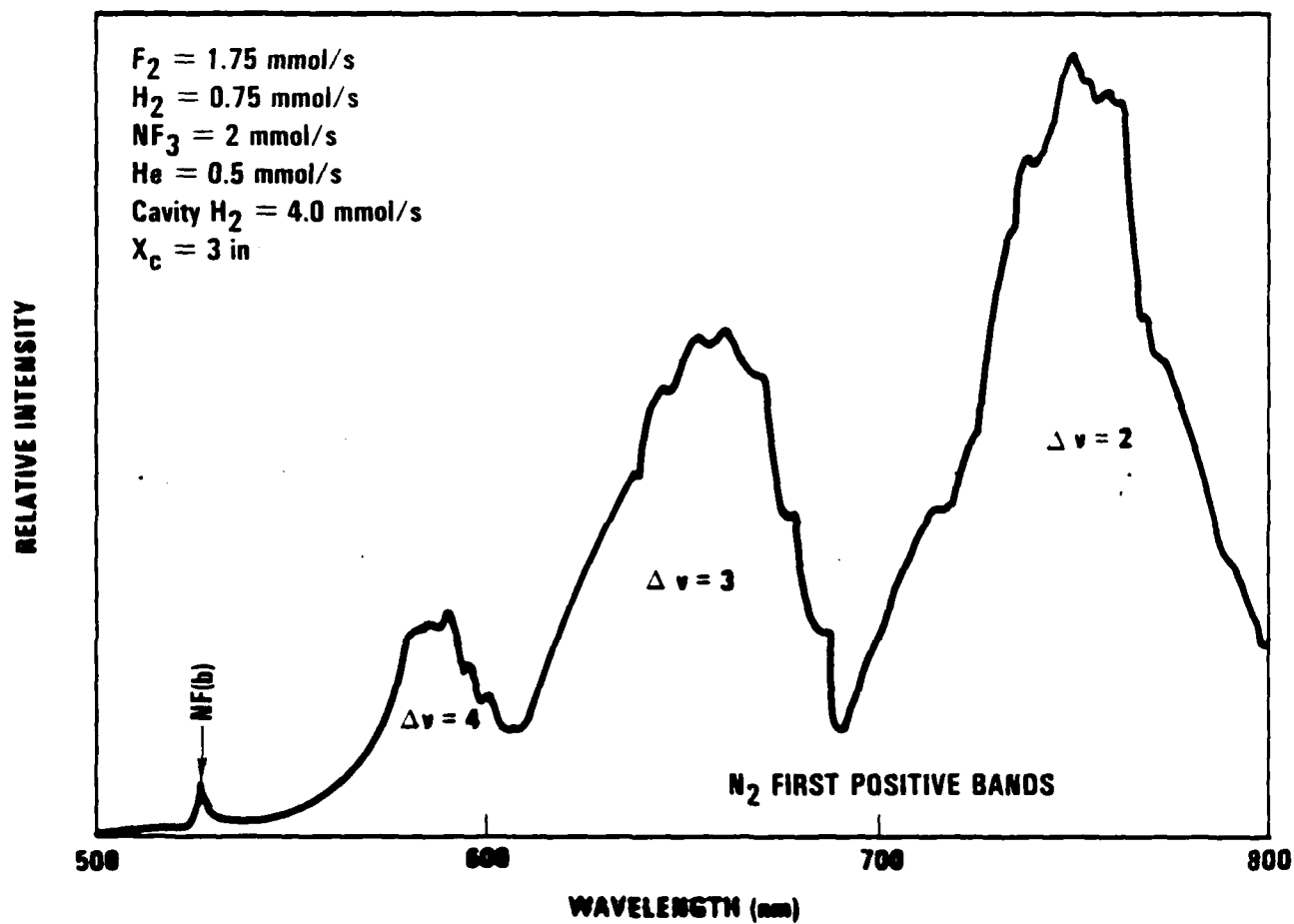


Figure 15. Tracor Northern spectrum from 500 to 800 nm corrected for instrument response.

Consequently, some of the data presented in this section represents a collection of 4 or 5 spectra which could not be differentiated from one another. A typical photograph of the chemiluminescence is shown in Figure 16. This shows a dark region in the center of the cavity. Using a video camera, conditions were found where this dark spot could be minimized. However, this did not appear to change the integrated excited state density.

The question arises on how to relate the data collected to excited state densities. As can be seen from the photograph, the flame is diffuse. The diagnostics were originally intended to sample a localized volume ($\sim 0.0126 \text{ cm}^3$) in the flow field and to scan exclusively along the flow direction, X_c . Hence, attempts to scan the spectrometer in the horizontal direction were minimal. Thus, number densities were obtained only for a given position. To obtain a yield of $N_2(B)$, i.e., the number of excited species produced per NF_2 molecule of flow, an integrated number is needed. The intensity variations in the horizontal direction were estimated from the video tapes and from still photographs of the flame and used to obtain the average density in a given X_c plane.

A standard flow condition was set by fixing the N_2F_4 flow and varying the other flows to obtain optimum $N_2(B)$ emission. The combustor was initially set to run with He diluent. However, all tests showed emission decreased when He was added. Consequently, all subsequent tests were run without the He. A parametric plot of relative $N_2(B)$ intensity versus combustor F_2 is shown in Figure 17 for the F_2 to H_2 ratio kept at 1.7 to 1. There was very little dependence of emission on this variable. Variation of the F_2 to H_2 ratio over a reasonable range of around 2 also showed little effect on the $N_2(B)$ density. A parametric plot of $N_2(B)$ intensity versus cavity H_2 is shown in Figure 18. This showed a relatively strong peak near a H_2 flow of 3 mmol/s. Based on the above parametric studies, the flow condition chosen as nominal was:

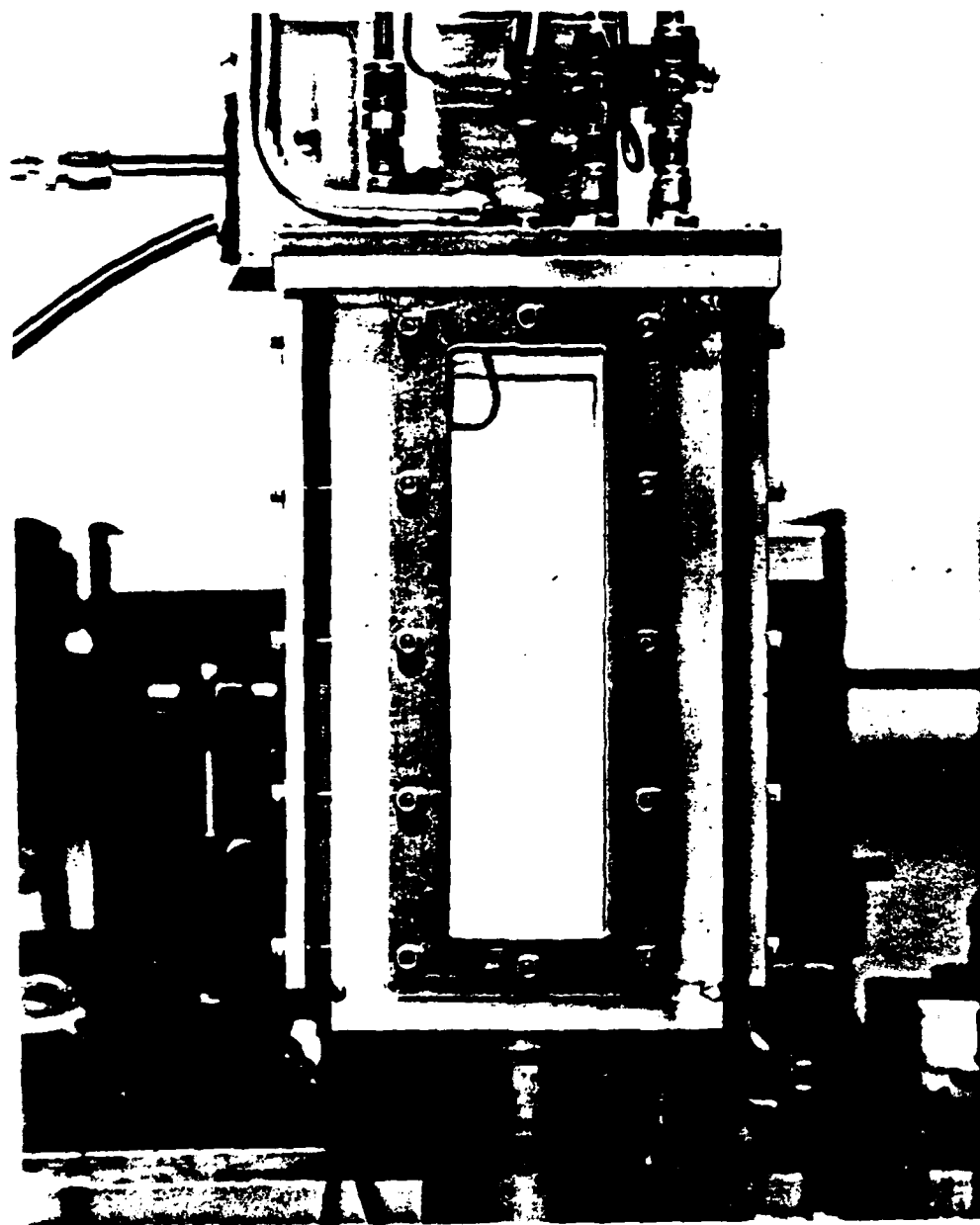


Figure 16. Photograph of N_2 ($B \rightarrow A$) chemiluminescence.

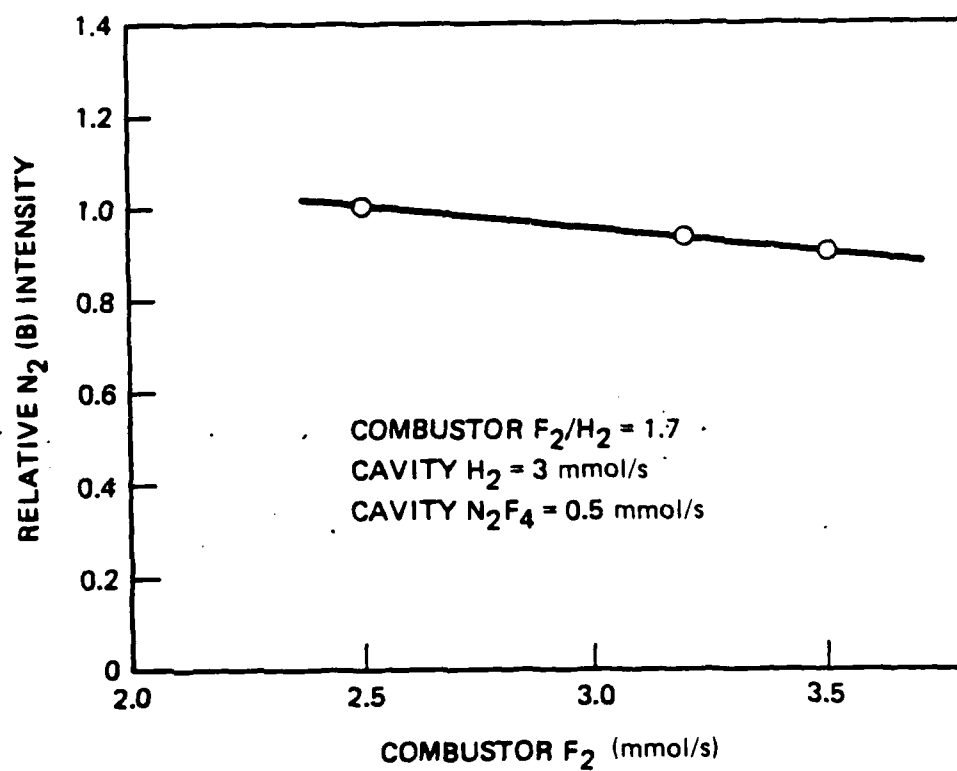


Figure 17. Plot of $N_2(B)$ emission versus combustor fluorine.

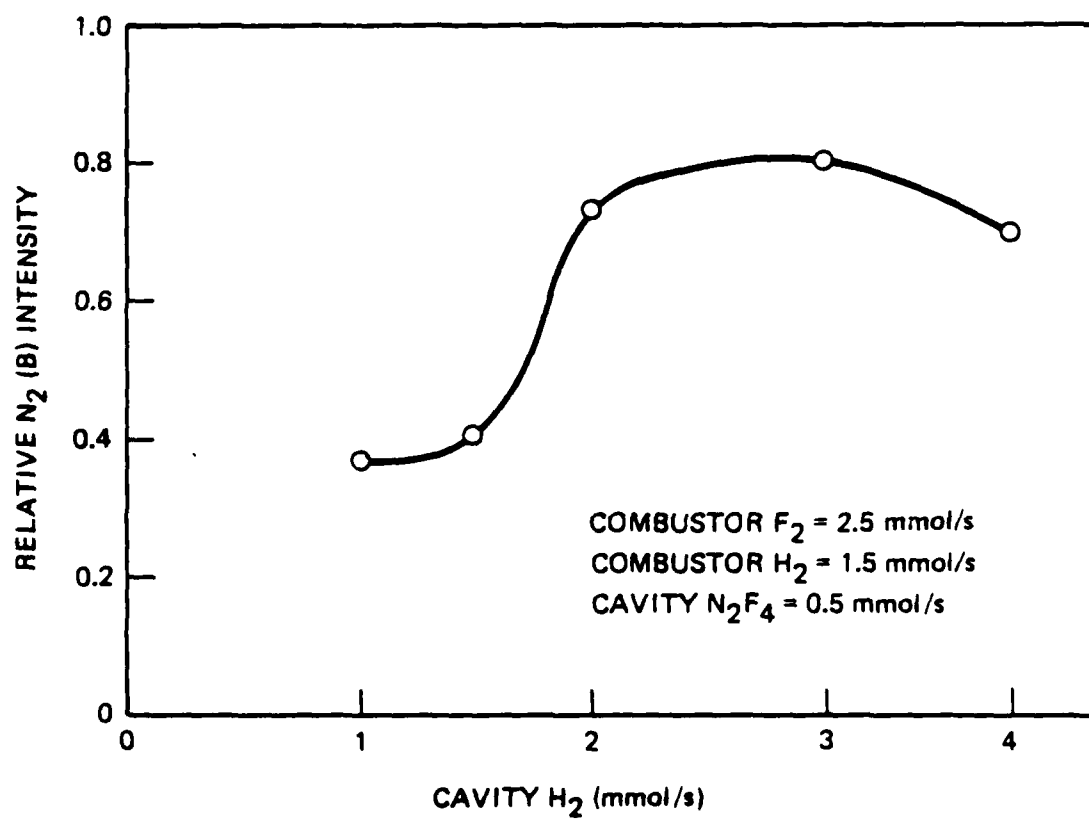


Figure 18. $N_2(B)$ density versus cavity H_2 .

combustor F_2 = 3.2 mmol/s
 combustor H_2 = 1.9 mmol/s
 cavity H_2 = 3.0 mmol/s
 cavity N_2F_4 = 0.5 mmol/s
 cavity pressure = 1.0 torr*
 combustor pressure = 90.0 torr

The orifice size of the second set of injection holes in the nozzle limited the flow of N_2F_4 to 0.6 mmol/s. The N_2F_4 was subsequently added through the bottom set of injector holes which allowed higher flow rates of N_2F_4 .

In most initial tests, the diagnostics were lined up to observe the center of the cavity. Later, when photography showed the dark region in the center of the cavity, the diagnostics were repositioned to look at the bright side regions. A factor of 6 increase in intensity was observed in moving from the center of the flow to the side. A plot of the number densities of various species versus X_c for the standard flow condition in the brightest part of the flame is shown in Figure 19. These densities apply for the brightest part of the flame. In reality, the intensity profile across the cavity is as shown in Figure 20.

The yield of a particular excited species, Y^* , can be approximated by the expression

$$Y^* = N^* \times v \times A / (NF_2 \text{ flow}) \quad (10)$$

where N^* is the average density of the excited species of interest, v is the flow velocity and A is the cross sectional area. If the X_c at which the maximum emission occurs is used to compute a yield, the N^* for

* 1.00 torr = 133.322 Pa

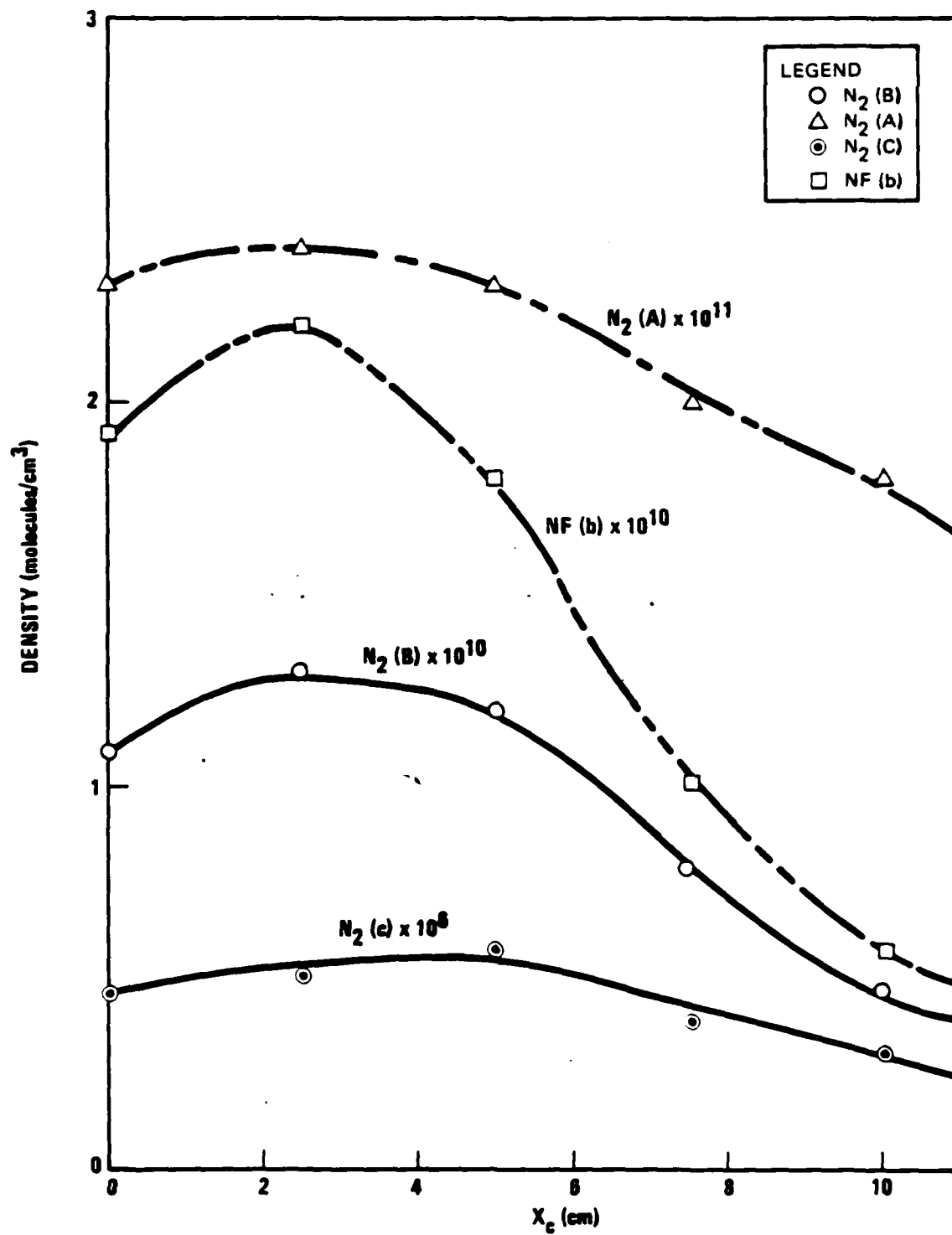


Figure 19. Plot of species densities versus X_c for H/NF_2 flame.

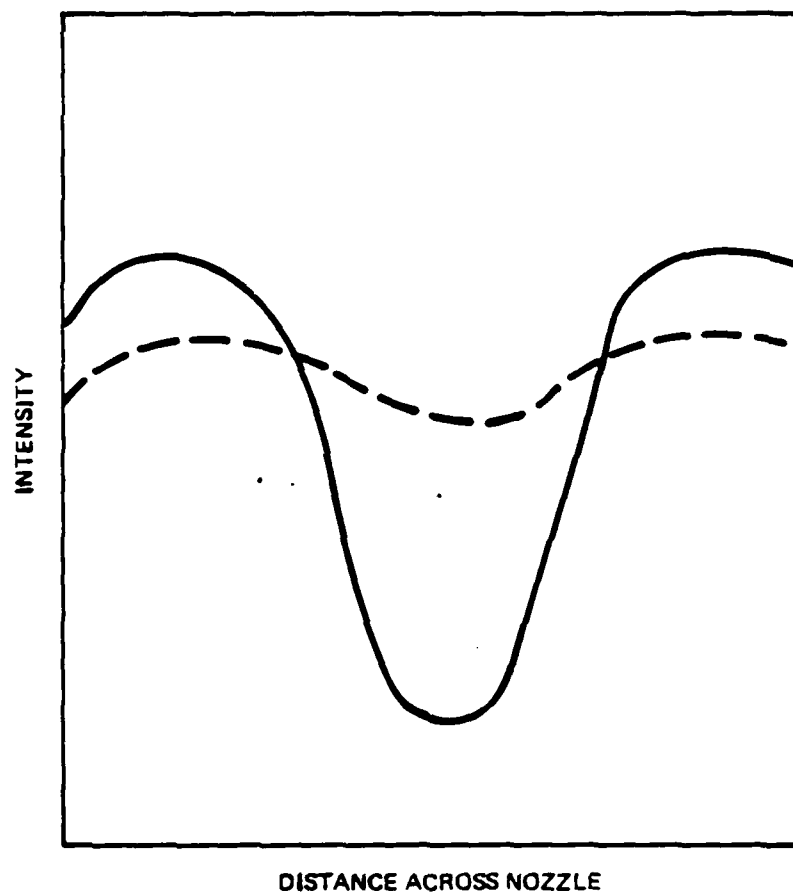


Figure 20. Intensity of $N_2(B)$ emission across nozzle. Solid line corresponds to region near nozzle. Dotted line is approximately 10 cm from bottom of nozzle.

the H/NF_2 runs (estimated from Figures 19 and 20) is approximately 1.4×10^{11} molecules/cm³. The flow from the nozzle is approximately Mach 4 giving a velocity of 4×10^5 cm/s. The cross sectional area is approximately 2.5×4 cm. With an NF_2 flow of 1 mmol/s (which assumes complete dissociation of the N_2F_4), a yield of 2.3×10^{-4} for $\text{N}_2(\text{A})$ is calculated. A yield of 1×10^{-4} for $\text{N}_2(\text{B})$ is calculated using the same assumptions.

NO was added to the flame to determine if it could be used as a detector of $\text{N}_2(\text{A})$. The transfer rate from $\text{N}_2(\text{A})$ to NO is known to be fast ($\sim 1 \times 10^{-10}$ cm³ molecule⁻¹ s⁻¹) so it appears that an estimate of the $\text{NO}(\text{A})$ density could be used to infer the amount of $\text{N}_2(\text{A})$ present. Addition of NO did result in suppression of the N_2 emissions and the appearance of a pinkish flame. $\text{NO}(\text{A} \rightarrow \text{X})$ emission was observed using a Princeton Applied Research Optical Multichannel Analyzer (OMA 1). Quantitative data (as a detailed function of NO flow) was not recorded. However, it was observed that flows up to 2 mmoles/s resulted in increased $\text{NO}(\text{A} \rightarrow \text{X})$ emission. The intensity of the $\text{NO}(\text{A} \rightarrow \text{X})$ emission was up a factor of approximately 20 from the background NO emission with 2 mmoles of added NO . Qualitatively, the increase in $\text{NO}(\text{A} \rightarrow \text{X})$ emission with increasing NO flow was gradual with no clear endpoint observed. Also, the NO was not mixed well with the flow, making this test unclear.

Combustor calorimetry was performed for the optimum condition. The calorimetry measurement consisted of measuring the difference in temperature between the input and output combustor cooling water flow for a known flow rate of cooling water. The raw calorimetry data showed a temperature change of 4.63 K for a water flow of 0.62 gal/min. This gives a heat loss to the combustor walls of 183.5 cal/s. The heat available from burning F_2 and H_2 in the combustor is 247 cal/s. This indicated that there were 63.5 cal/s available for both heating the gas and dissociating the F_2 into F-atoms. A calculation in which this heat is partitioned into heating and dissociation gives an F-atom flow from the combustor of approximately 1.4 mmol/s. This is about half of the fluorine that would be expected if the reaction



went to completion.

Infrared spectra of HF chemiluminescence were run to determine the cavity temperature as a function of position for the flow condition tabulated above. The temperature results are summarized in Table 3.

Table 3. CAVITY TEMPERATURE AS A FUNCTION OF FLOW DISTANCE

X_c (cm)	Temperature (K)
3	1000
6	1150
9.5	1250

In all the tests the device was run with maximum pumping and no window purges which resulted in low cavity pressures of the order of 1 torr. Attempts were also made to vary the cavity pressure to determine if emission intensities could be changed. The first way was to add Argon purge flow to the side windows. This changed the appearance of the flame, tending to push it toward the center. However, it did not appear to change the total integrated intensity of $\text{N}_2(\text{B})$ emission. The second way was to throttle the pumps to increase the cavity pressure. This had the effect of pushing the flame up into the nozzle, resulting in much of the cavity being dark. These attempts indicated that major hardware modifications would be needed to adjust flows, uniformly condense the flame and increase the cavity pressure. In fact, in some early tests, aluminum shrouds were added to the cavity spaced approximately 2 cm apart to contain the flow. This resulted in a uniform flame with few variations in either flow or width direction. Although not completely quantified, the conclusion was that any attempts to contain the flow resulted in the same integrated density of excited species in a given plane, even though it could produce higher local densities.

3.2.2 NF_3 Based System

Because of the limited supply of N_2F_4 currently available, some tests were run with NF_3 . This was motivated by the following reasons: First, NF_3 is available in virtually unlimited supplies and has relatively safe handling characteristics, whereas N_2F_4 is in short supply and is dangerous and unstable. Previous HF and IR&D tests showed that the characteristic $\text{N}_2(\text{B})$ and $\text{NF}(\text{b})$ emissions were present when HF lasers were run with NF_3 as a combustor fuel. In addition, thermodynamic calculations indicate that large concentrations of NF_2 radicals can be produced in the combustor if it is operated at the appropriate temperature. Finally, it should be easier to mix H_2 into an F, NF_2 stream (since this is routinely done with conventional CW HF chemical lasers) than to mix a heavy species, NF_2 into the F, HF combustor stream.

The procedure used to optimize $\text{N}_2(\text{B})$ emission in an NF_3 based system was to set the $\text{N}_2(\text{B})$ diagnostic to look at a particular X_c . A combustor condition chosen on its likelihood to produce NF_2 radicals was then set. Diluent was adjusted to give the brightest and most uniform flame. The cavity hydrogen was then adjusted to give the brightest flame at that X_c . The distance, X_c , was then scanned. The combustor condition was then changed and the procedure repeated. Finally X_c was changed and again the procedure was repeated.

Some observations of $\text{N}_2(\text{B})$ intensity are shown in Figures 21 through 27. Figure 21 shows a plot of $\text{N}_2(\text{B})$ as a function of X_c when the flows were optimized near the nozzle. Figure 22 shows the same plot when the optimization occurred at an X_c of 7.6 cm. Figure 23 shows a plot of $\text{N}_2(\text{B})$ as a function of cavity hydrogen. Cavity pressure is shown as the dotted line in the figure. Figure 24 shows a similar plot at a slightly different combustor condition. Figure 25 shows a plot of $\text{N}_2(\text{B})$ density as a function of fluorine flow for the other conditions listed in the figure. Figure 26 shows a plot of $\text{N}_2(\text{B})$ versus combustor H_2 for the conditions listed in the figure. Finally Figure 27 shows a plot of $\text{N}_2(\text{B})$ density versus cavity pressure. In this figure, the cavity pressure was raised by throttling the vacuum pumps.

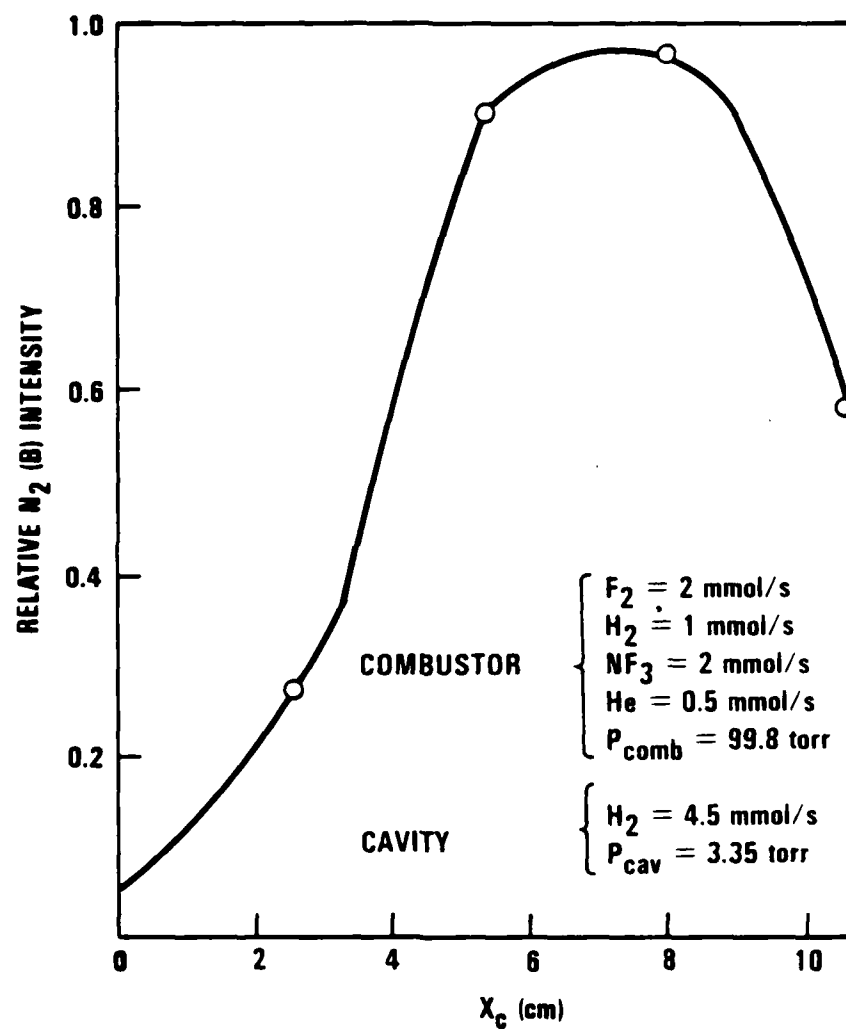


Figure 21. $N_2(B)$ intensity versus distance from nozzle. $N_2(B)$ optimized near nozzle.

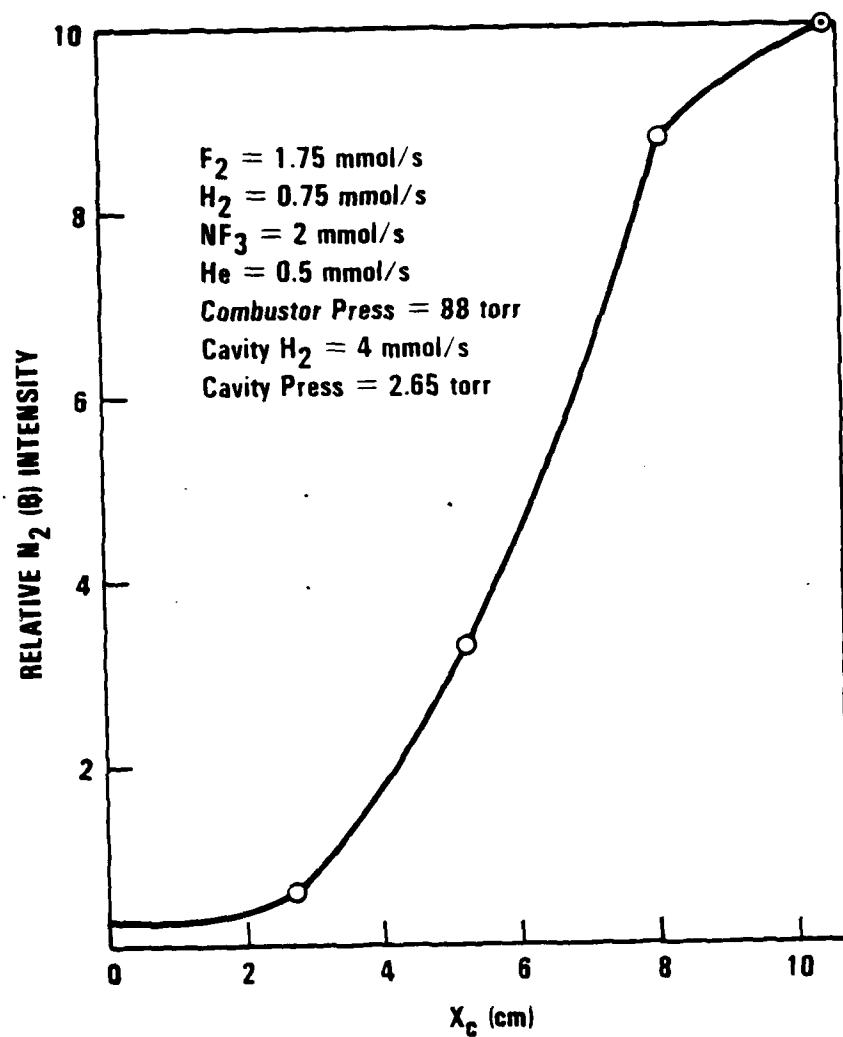


Figure 22. $N_2(B)$ versus X_c , $N_2(B)$ optimized at $X_c = 7.6$ cm.

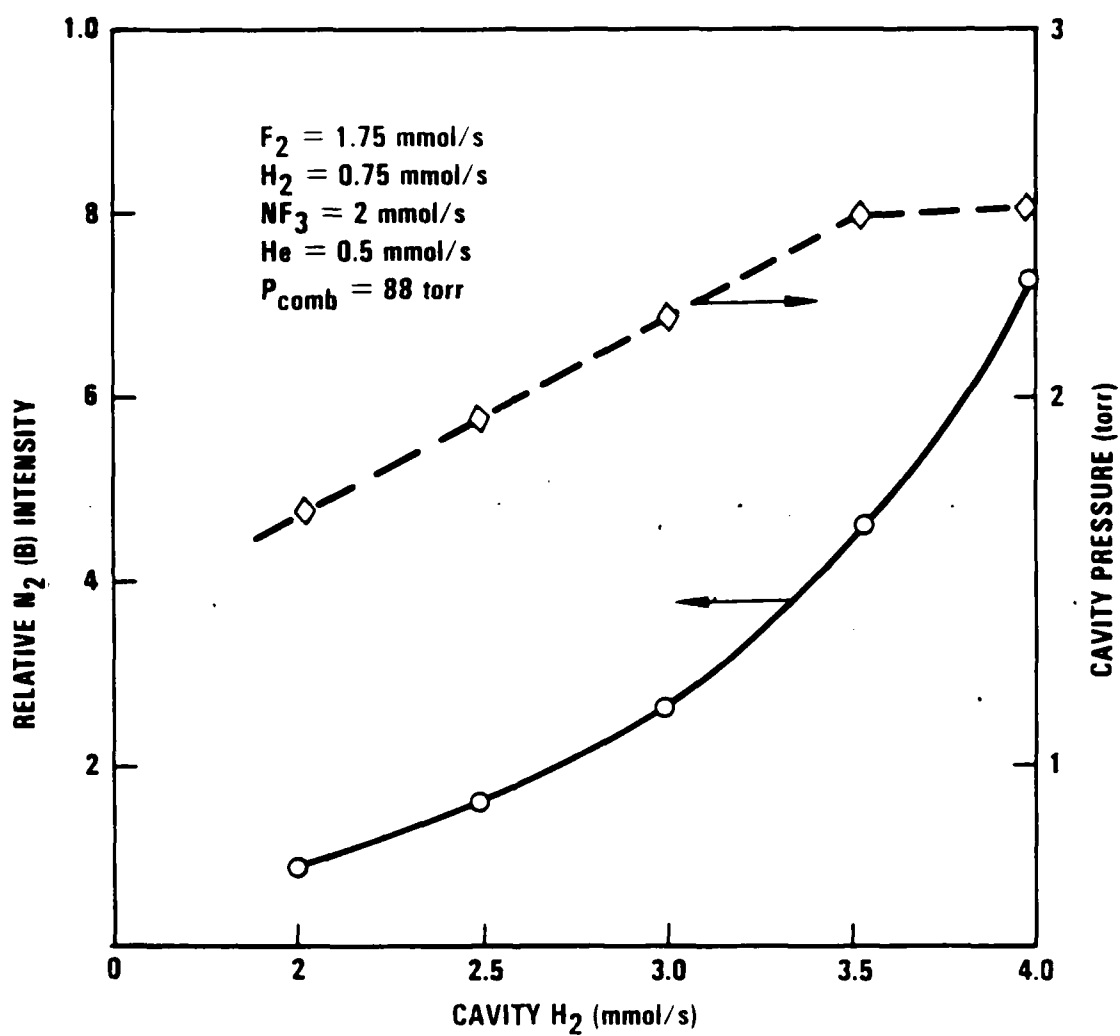


Figure 23. $N_2(B)$ versus cavity H_2 .

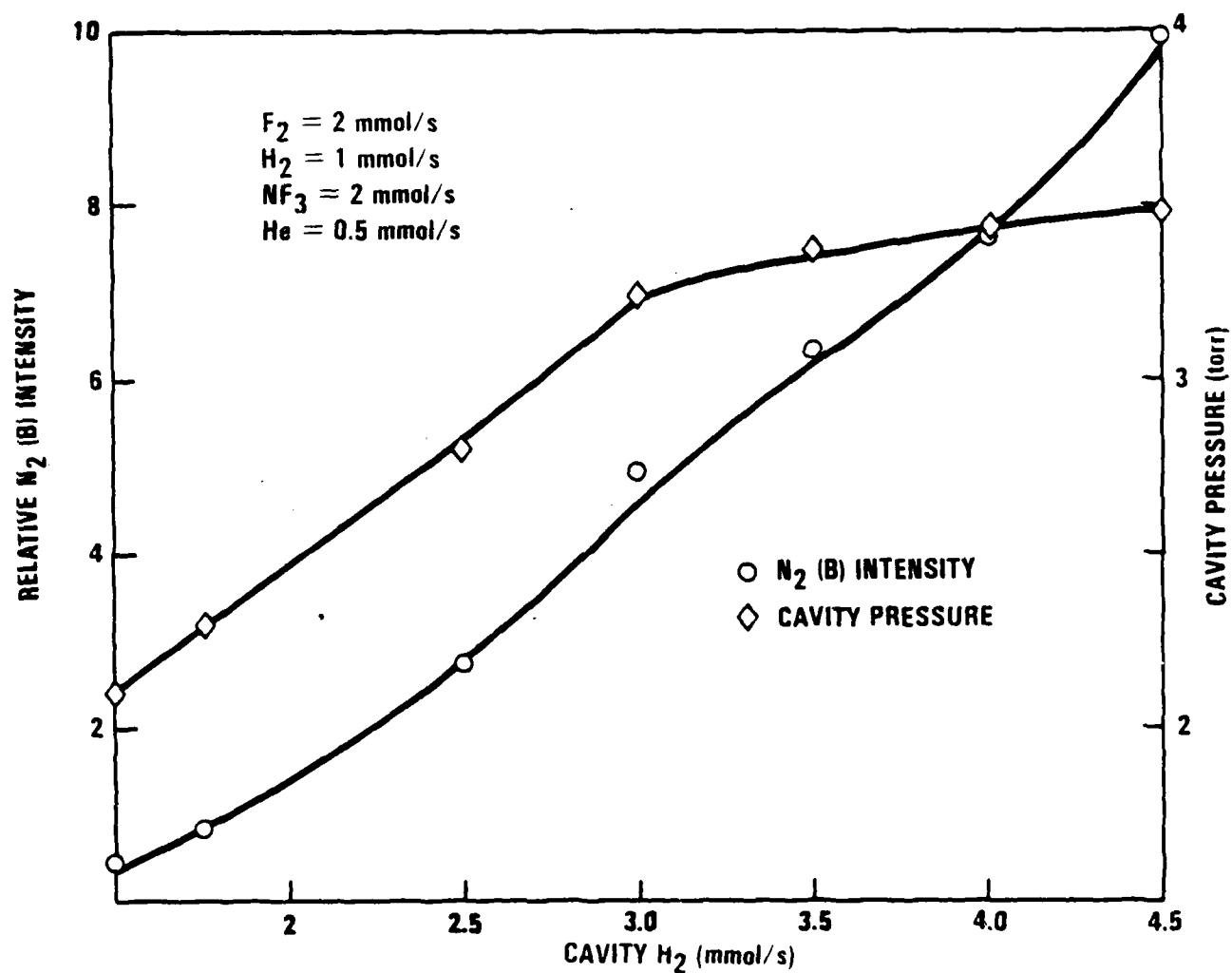


Figure 24. $N_2(B)$ versus cavity H_2 .

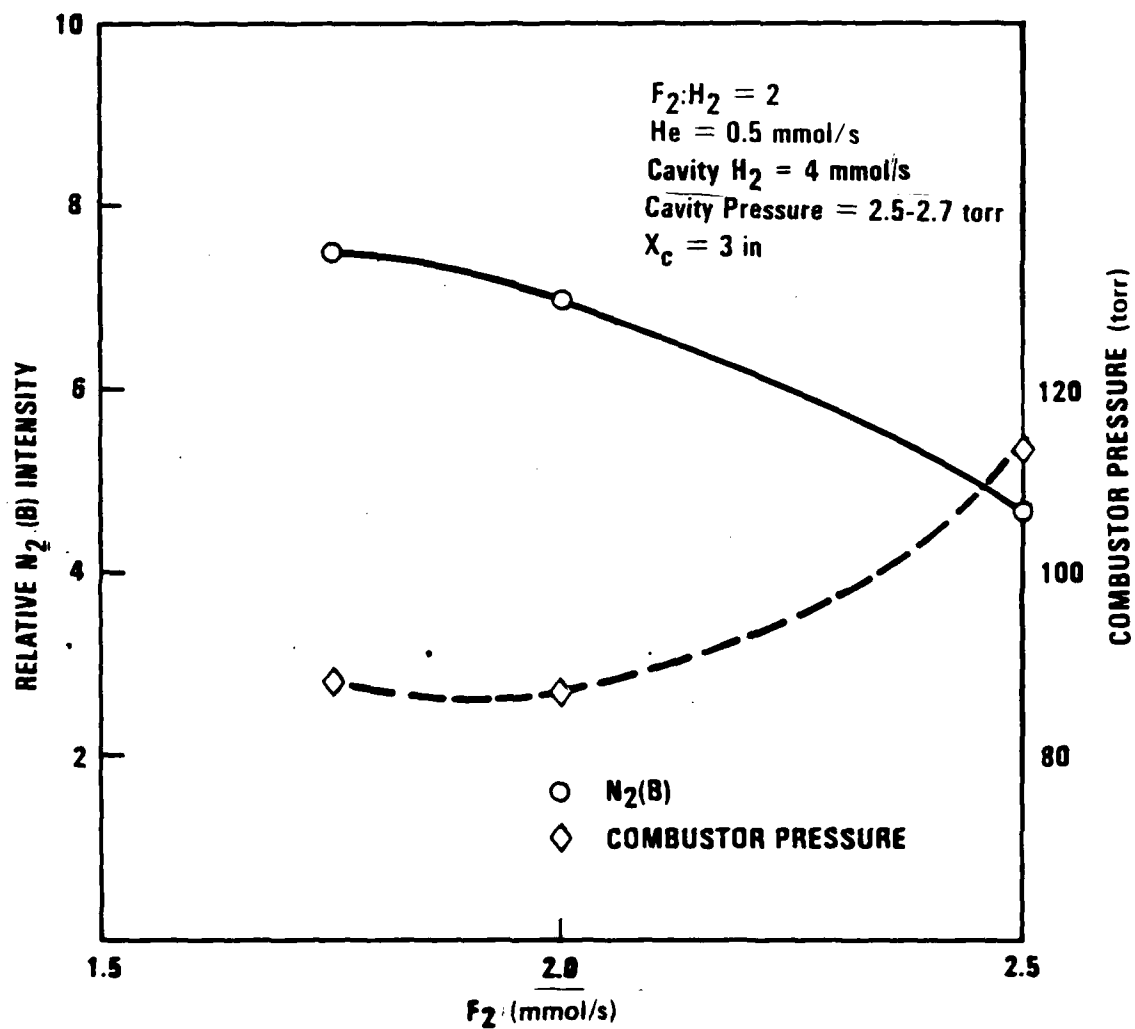


Figure 25. $N_2(B)$ versus F_2 flow with the F_2/H_2 ratio constant.

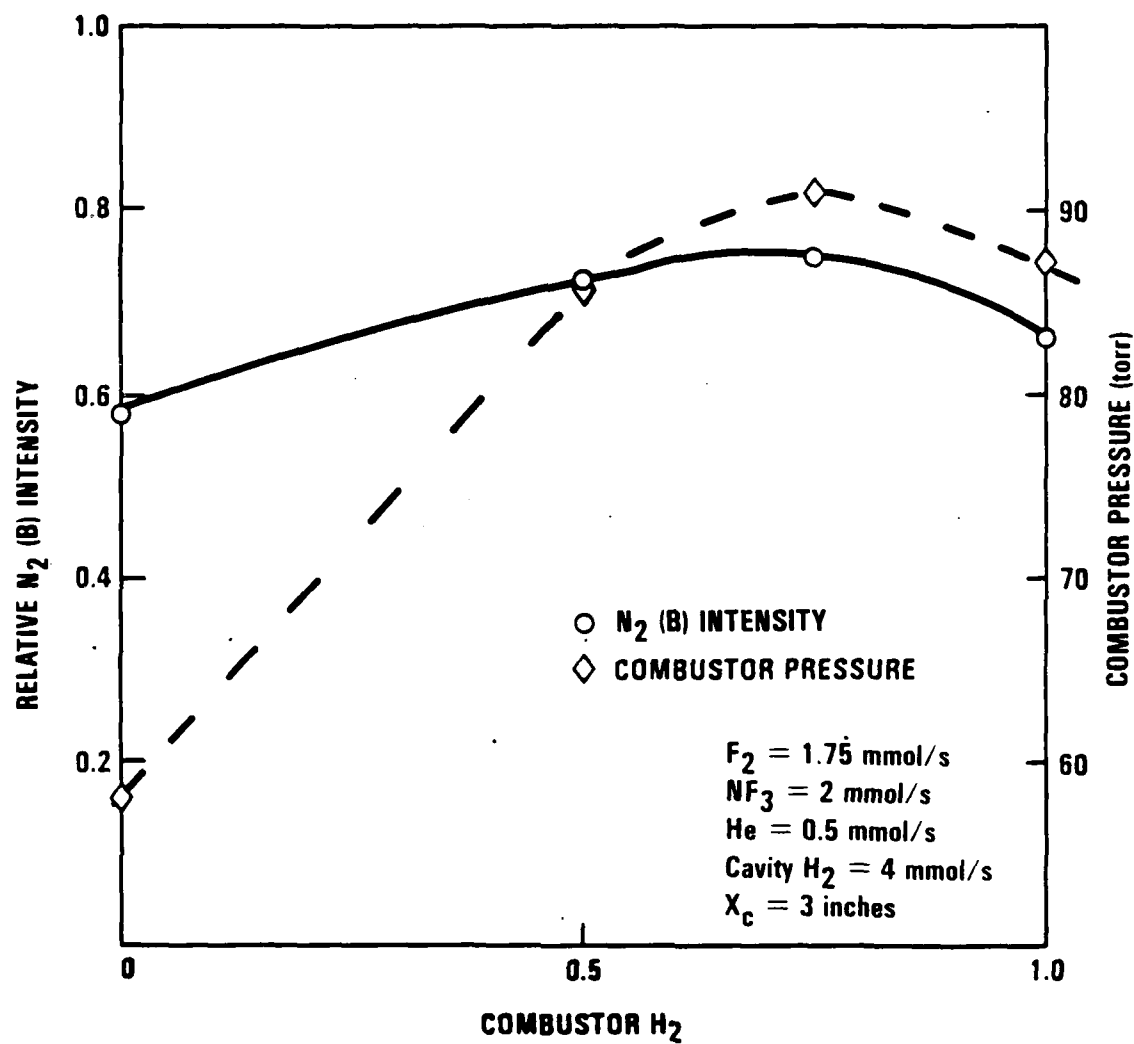


Figure 26. $N_2(B)$ versus combustor H_2 .

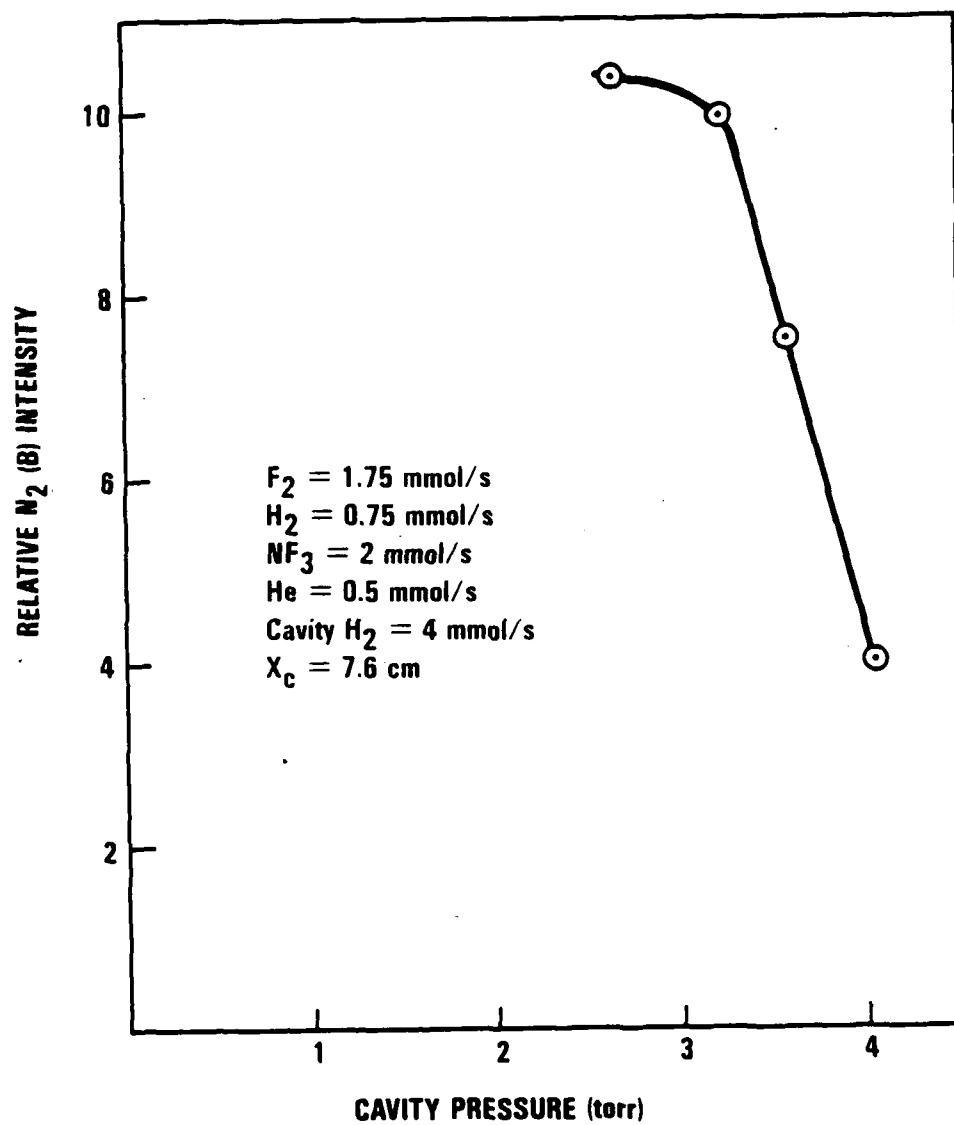


Figure 27. $N_2(B)$ density versus cavity pressure

HF chemiluminescent spectra were taken to determine the cavity temperature. Plots of relative number density versus $J(J+1)$ are shown in Figure 28. This plot gives a cavity temperature of near 1800 K.

An apparant change in the $N_2(B)$ vibrational state distribution was also observed during these runs manifesting itself as a change in peak height ratios for different flow conditions. The two spectra in Figure 29 show the magnitude of the observed change. The upper spectrum had flow rates of $F_2 = 1.75$ mmol/s, combustor $H_2 = 0.87$ mmol/s, $NF_3 = 3$ mmol/s, cavity $H_2 = 3$ mmol/s and He = 0.5 mmol/s. The combustor pressure was 88 torr while the cavity pressure was 2.18 torr. The spectrum was taken at a position 7.5 cm from the nozzle exit plane. The lower spectrum had flow rates of $F_2 = 1.75$ mmol/s, combustor $H_2 = 0.75$ mmol/s, $NF_3 = 2$ mmol/s, cavity $H_2 = 4$ mmol/s and He = 0.5 mmol/s. The combustor pressure was 89 torr while the cavity pressure was 3.25 torr. The spectra in these figures were not corrected for spectral response and demonstrate the enhanced sensitivity of the detector at shorter wavelengths.

The plots in Figures 21-27 were all normalized to the most intense flame observed. For this condition, the following flows and excited state densities were observed.

FLOWS

F_2	2 mmol/s
Combustor H_2	1 mmol/s
Cavity H_2	4 mmol/s
Combustor NF_3	2 mmol/s
Helium	0.5 mmol/s

EXCITED STATE DENSITIES

$N_2(B)$	$\approx 9 \times 10^{11}$ molecules/cm ³
$N_2(C)$	$\approx 7 \times 10^7$ molecules/cm ³
$N_2(A)$	$\approx 2 \times 10^{12}$ molecules/cm ³
$NF(b)$	5×10^{11} molecules/cm ³

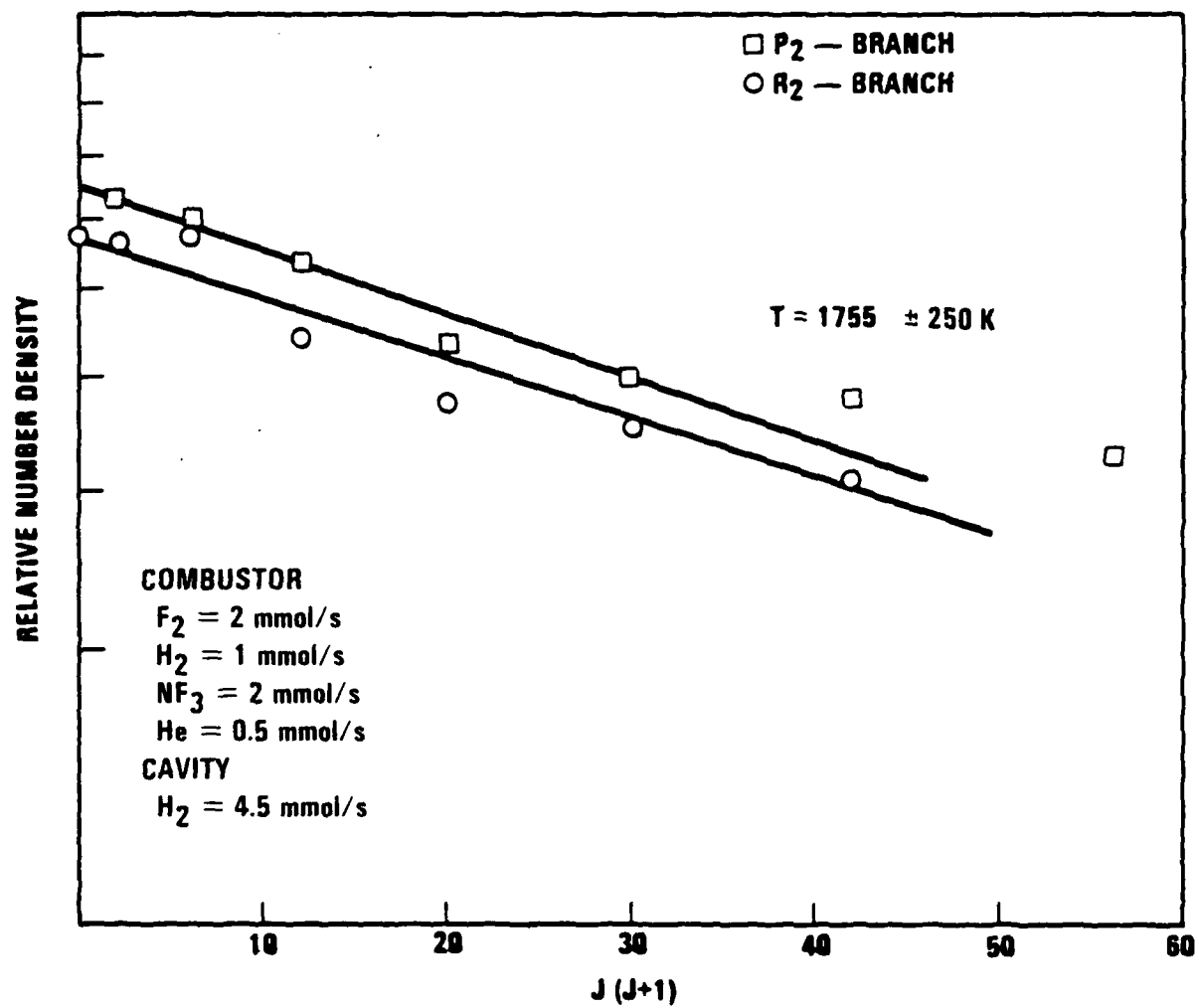


Figure 28. HF chemiluminescence temperature determination

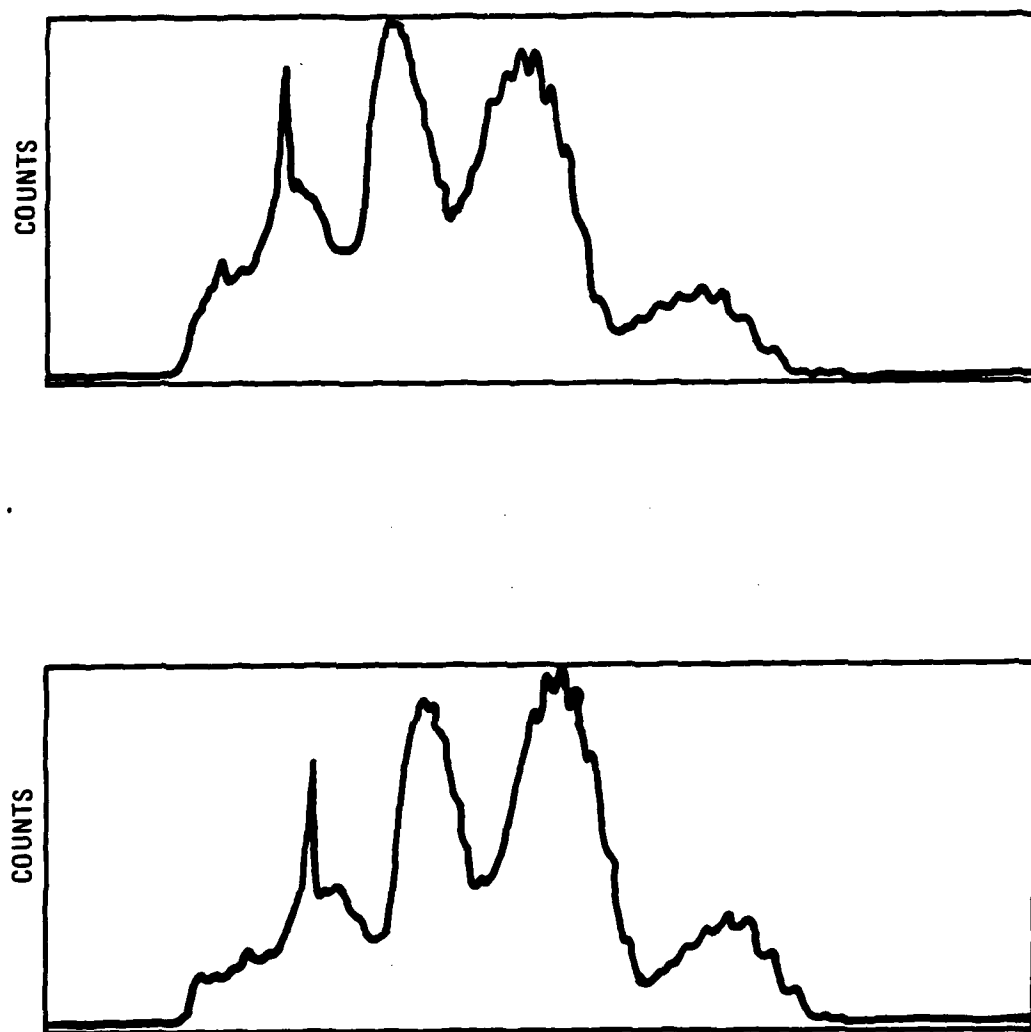


Figure 29. Spectra of $\text{H}_2/\text{F}_2/\text{NF}_3$ system showing change in $\text{N}_2(\text{B})$ vibrational distribution.

PHYSICAL PARAMETERS

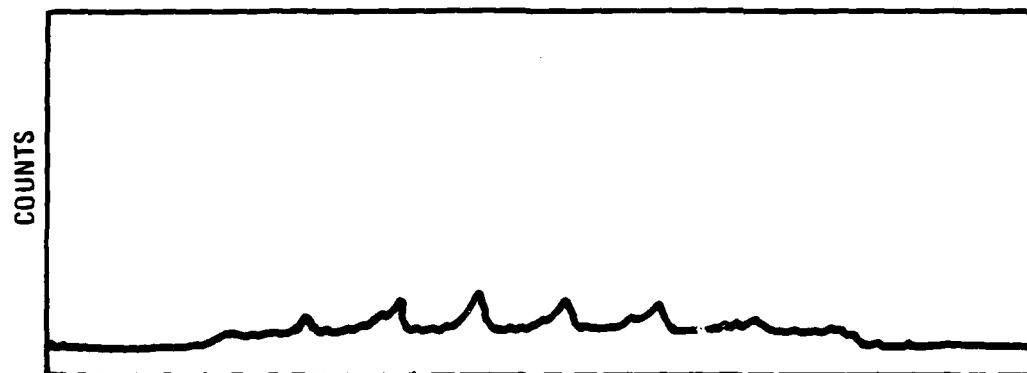
Combustor Pressure 88 torr
Cavity Pressure 2.65 torr
Gas Temperature (1750 ± 200) K

The highest observed excited nitrogen densities occurred in the system where NF_3 was run in the combustor. However, a test run where the H_2 in the combustor was totally shut off (Fig. 26) indicates that little, if any, chemistry was occurring in the combustor and that the observed emissions were a direct result of reaction of NF_3 , H_2 and F_2 in the cavity. The high temperatures (1700 to 2200 K) in the excited state production region and the fact that emission intensities peak far downstream of the mixing region also support this conclusion.

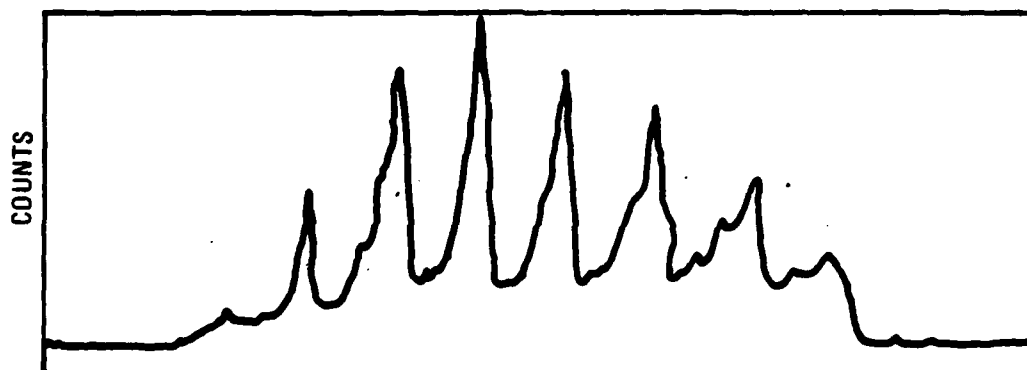
Addition of NO also confirmed this hypothesis. Whereas, in the H/NF_2 system, addition of NO resulted in the gradual buildup of $\text{NO}(\text{A} \rightarrow \text{X})$ emission, in this system little $\text{NO}(\text{A})$ was formed indicating that the NO was reacting with an intermediate, possibly $\text{N}({}^2\text{D})$. NO spectra are shown in Figure 27 for no added NO, for 0.15 mmol/s added NO and for 0.54 mmol/s added NO. The $\text{NO}(\text{A} \rightarrow \text{X})$ spectrum appears to peak at the 0.15 mmol/s flow.

Attempts to run the combustor at higher flows to increase the combustor temperature and, hence, NF_2 concentration were largely unsuccessful. This may have been due to a heat loss problem in the combustor.

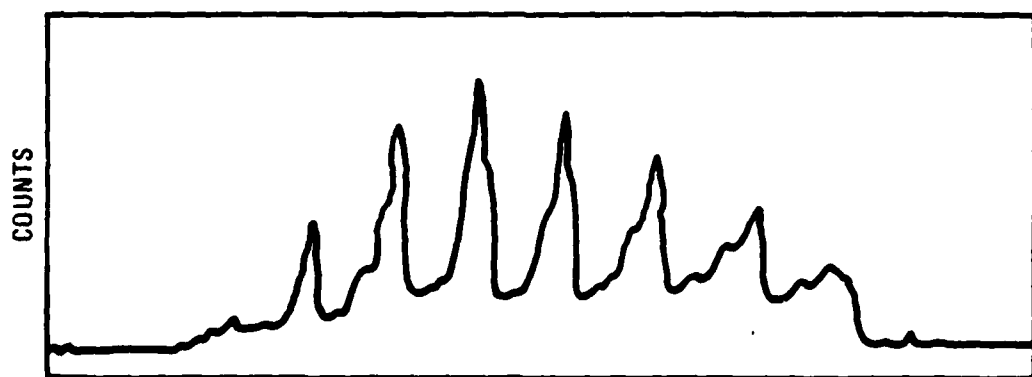
This was substantiated by observation of $\text{N}_2(\text{B})$ emission in an HF laser device with a 10 cm gain length HYLTE mixing nozzle where NF_3 was used as the combustor fuel. This test was conducted piggyback on another program's experiments so there was no flexibility to optimize the N_2 excited state emissions. In this experiment, the temperatures in the cavity were much lower (near 500 K) and the flow was more confined due to a better match between combustor and nozzle. The emission in this



(a.) No added NO



(b.) 0.14 mmol/s NO



(c.) 0.54 mmol/s NO

Figure 30. NO(A-X) spectrum.

experiment appeared greener to the eye than the penthouse experiments. A spectral scan confirmed that the NF(b) emission was higher in proportion to the N₂(B) emission than in the penthouse experiments. The estimated N₂(B) densities in that system were somewhat lower than those seen in the penthouse H/NF₂ experiments. The different character of the flame supports the conclusion that the observed flame in the penthouse was the result of a direct reaction between F₂/H₂/NF₃ and not the result of F-atoms and NF₂ being formed in the combustor with the subsequent reaction with H₂ to initiate the H/NF₂ chemistry.

3.2.3 H/NF₃ System

A test was conducted in which NF₃ was injected into the cavity instead of N₂F₄. A bright yellow flame similar to that obtained with N₂F₄ in the cavity was observed. The flame appeared more uniform when observed on the video tape than did the N₂F₄ emission. This could be because higher flow rates produced better mixing in the NF₃ system. A quick optimization of the N₂(B) emission was made. The flows at which the brightest N₂(B) emission was observed were

Combustor F ₂	5 mmol/s
Combustor H ₂	3 mmol/s
Cavity H ₂	4 mmol/s
Cavity NF ₃	2.4 mmol/s
Cavity Pressure	2.0 torr
Combustor Pressure	137 torr

Plots of concentrations of excited states, N₂(B), N₂(A), N₂(C) and NF(b), versus X_c for the optimum flow condition are shown in Figure 31.

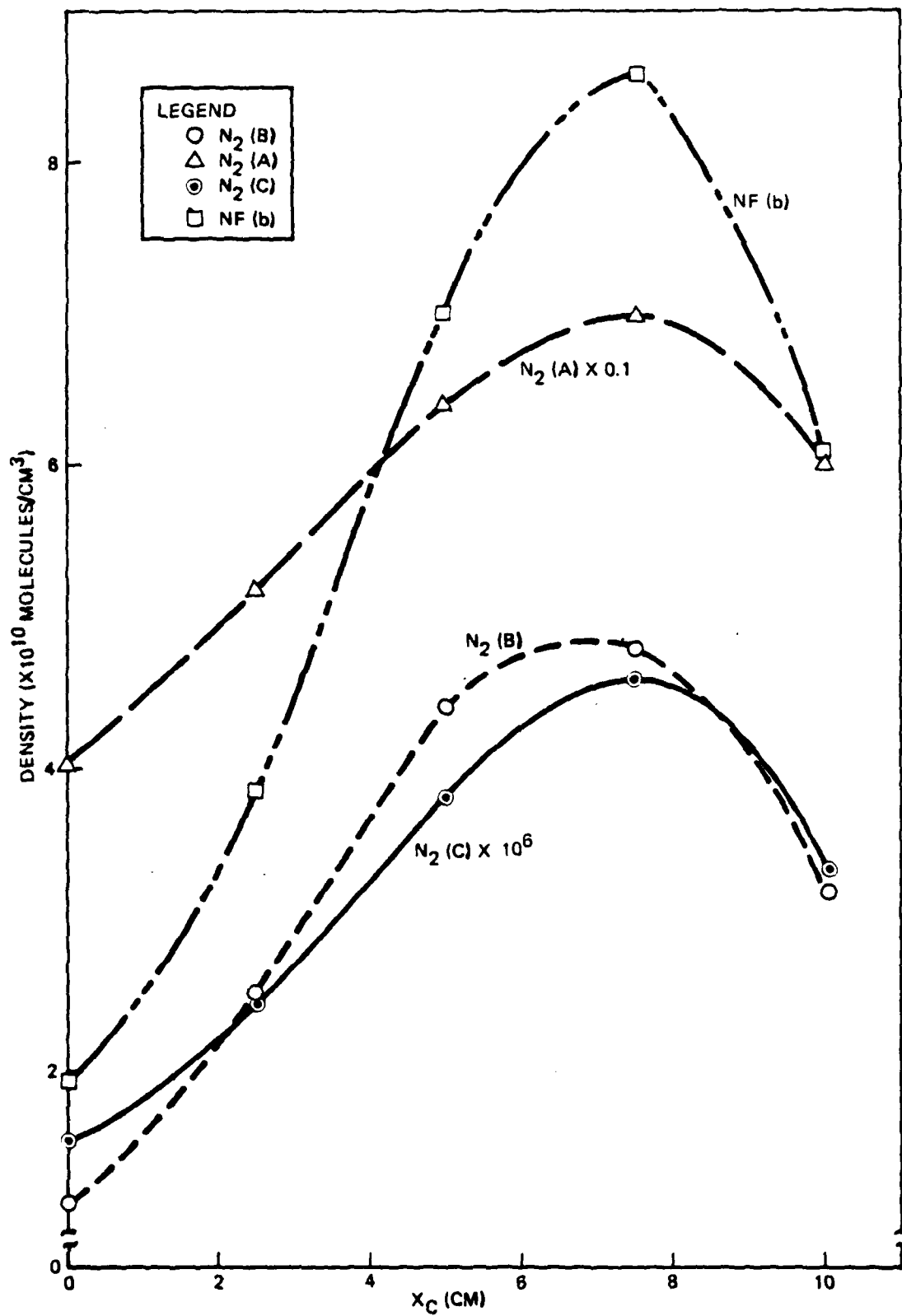


Figure 31. Plots of excited state concentration versus X_C .

4. DISCUSSION OF RESULTS

4.1 H/NF₂ RESULTS

As described in paragraph 3.2.1, the tests conducted with F-atoms issuing from the combustor mixed with N₂F₄ downstream were relatively insensitive to almost all flows. Also, the highest yields of 2.3×10^{-4} for N₂(A) and 1×10^{-4} for N₂(B) are much lower than were expected at the beginning of the contract. There are two factors that could contribute to the low yields in these experiments: fluid mechanics and chemistry.

The mixing hardware used in these experiments was developed for HF/DF chemical lasers. The combustor was designed to run at even higher flows than were used in these experiments which may have limited the yield of F-atoms. The lower flows account for the fact that best performance was achieved with no diluent in the system. The mixer was designed to mix hydrogen or deuterium into an F-atom stream. In its HF/DF laser configuration, H₂/D₂ was mixed in the first and third ports while helium was added in the second port to aid in mixing. In some experiments with this nozzle, two nozzle banks were run making a set of six injectors with alternating flows of H₂ and diluent. An attempt was made to mix a heavier species, NF₂, into the stream than the nozzles were designed for. The diffuse nature of the flame indicated that the combustor expansion nozzle and the mixer were not well matched. However, experiments conducted with similar hardware did not produce appreciably higher yields of excited nitrogen.

A similar nozzle system has been used to mix bromine into an H-atom flow to produce an HBr laser. These tests showed that the nozzles were not effective in mixing in a heavy species like Br₂. Part of the reason for the low yields was an inadequately designed mixing system for the species of interest. However, it appears that improved mixing would probably increase densities by at most a factor of 10. This still produces a relatively low yield of excited nitrogen, indicating that there is a contributing factor in the chemistry. It was beyond the scope of the

current contract to perform kinetic analysis of these experiments, but it appears that either some kinetic rate in the formation chain was slow or that some species was effective in quenching excited state nitrogen production. This should be examined in more detail with a kinetics model.

4.2 NF_3 BASED SYSTEM

A thermodynamic analysis of the combustor used in the NF_3 experiments indicated that the combustor with NF_3 added was running at a temperature as low as 500 K. At this temperature, only small amounts of NF_2 or F-atoms were being formed in the combustor. Consequently, it appears that the observed emissions were coming from an $\text{H}_2/\text{F}_2/\text{NF}_3$ flame in the cavity. This is substantiated by the high temperatures observed in the cavity of this device. Thus, even though the brightest $\text{N}_2(\text{B})$ emission was observed in this system, it probably was not under conditions of interest for using the nitrogen excited states as subsequent energy transfer partners. The experiment demonstrates that the flame is capable of producing high excited state densities.

REFERENCES

1. J. M. Herbelin and N. Cohen, "The Chemical Production of Electronically Excited States in the H/NF₂ System," Chem. Phys. Lett., 20, 605 (1973).
2. C. T. Cheah, M. A. A. Clyne and P. D. Whitefield, "Reactions Forming Electronically-excited Free Radicals, Part I. Ground State Reactions Involving NF₂ and NF Radicals," J. C. S. Faraday, II, 76, 711 (1980).
3. C. T. Cheah and M. A. A. Clyne, "Reactions Forming Electronically-excited Free Radicals Part 2. Formation of N-Atoms in the H + NF₂ Reaction and N-Atom Reactions," J. C. S. Faraday, II, 76, 1543 (1980).
4. C. T. Cheah and M. A. A. Clyne, "Reactions Forming Electronically-Excited Free Radicals Part 3. Formation of Excited Molecular States in the H + NF₂ Reaction," J. Photochemistry 15, 21 (1981).
5. J. A. Betts and D. J. Miller, Advanced Laser Concepts and Addendum, AFWL-TR-77-234, Air Force Weapons Laboratory, Kirtland AFB, N. Mex., January 1978.
6. J. M. Herbelin, D. J. Spencer and M. A. Kwok, "Scale-up of NF(a) Produced by the H + NF₂ System in a Subsonic CW Laser Device," J. Appl. Phys. 48, 3050 (1977).
7. G. E. Copeland, "Lifetimes of the v' = 0, 1, 2 Levels of the A²T⁺ Electronic State of NO," J. Chem. Phys. 56, 689 (1972).
8. D. E. Shemansky and N. P. Carleton, "Lifetime of the N₂ Vegard-Kaplan System," J. Chem. Phys., 51, 682 (1969).
9. W. H. Smith, "Lifetimes and Total Transition Probabilities of NH, SiH and SiD," J. Chem. Phys. 51, 520 (1969).

END

12-87

DTIC